# Theoretical investigation of favipiravir antiviral drug based on fullerene and boron nitride nanocages

Kamal A. Soliman [a],[*], S. Abdel Aal [a],[b]

[a] *Department of Chemistry, Faculty of Science, Benha University, P.O. Box 13518, Benha, Egypt*
[b] *Department of Chemistry, College of Science, Qassim University, Saudi Arabia*

## ARTICLE INFO

## ABSTRACT

Smart implementation of novel advanced nanocarriers such as functionalized $C_{24}$ and $B_{12}N_{12}$ nanocages is used supplement for antiviral activity 5-Fluoro-2-hydroxypyrazine-3-carboxamide (Favipiravir; Avigan; T-705), as treatment of COVID-19. The interaction energies of Favipiravir with perfect ($B_{12}N_{12}$ and $C_{24}$) and doped ($BC_{23}$ and $CB_{11}N_{12}$) nanocages were studied at temperatures equal to 310.15 K and 298.15 K using DFT. Our results have shown that the interaction of the Favipiravir (C═O group) with $BC_{23}$ and $CB_{11}N_{12}$ is more favorable than with the $C_{24}$ and $B_{12}N_{12}$ nanocages in the gas and aqueous environments.

Additionally, the natural bond orbital, the highest occupied molecular orbital (HOMO), the lowest unoccupied molecular orbital (LUMO), energy gap, chemical reactivity, molecular electrostatic potential, and thermodynamic parameters of the optimized structure have been examined. Furthermore, the UV–Vis and infrared spectroscopy have been evaluated for the investigation of the molecular orbitals Participated in the absorption spectrum of the Favipiravir before and after the interaction with the $C_{24}$, $BC_{23}$, $B_{12}N_{12}$, and $CB_{11}N_{12}$, sites at maximum wavelength utilizing the time-dependent density functional theory (TD-B3LYP and TD-CAM-B3LYP). The intermolecular interactions have been analyzed by non-covalent interactions (NCI) and also, the electron localization function (ELF) is discussed.

## 1. Introduction

The 2019 infection pandemic (COVID-19) of the coronavirus is a serious bio-safety that has a serious impact on global society and the economy. COVID-19 has prompted the interest of scientists to treat this disease with an effective drug. Due to the ability of the COVID-19 virus to undergo antigenic changes and drug resistance, a significant objective of medical science and health care systems is the search for novel antivirals. Several developing drugs have been examined against COVID-19 [1]; favipiravir is one of the drugs cited for action against RNA-viral infections of COVID-19 [2] as broad-spectrum inhibitors [3]. Experimental treatment with Favipiravir for COVID-19 [4,5] has been provided that preliminary evidence for the prevention of viral infection with SARS-CoV-2. Favipiravir drug (5-Fluoro-2-hydroxypyrazine-3-carboxamide (T-705; Avigan; Favipiravir) was first prepared by Shi et al. [6], however, the performance of COVID-19 medications is still being questioned to date [7]. Consequently, the smart implementation of nanoscience has given great attention to exciting applications in the medical field and pharmaceutical studies [8]. The drug delivery systems

are distinguished over free drugs in aspects such as selectivity, longer circulation time, and lower dosage with low side effects [9] and better therapeutic efficacy. Density functional studies were performed to the structure and energetics of the interaction of the drug pyrazinamide (PZA) with graphene-based nanomaterials using a noncovalent functionalization approach [10].

The synthesis and application of carbon and BN-nanocages has recently been of great interest as drug carriers or drug detectors due to their unique physical and chemical properties such as a great adsorbing capacity, high thermal stability, and low poisonous quality. First-principles calculations have been carried out on the effect of functionalization of $B_{12}N_{12}$ and $C_{24}$ nanocage using heteroatoms such as C- and B-doping [11]. Compared to defect-free nanocage surface ($B_{12}N_{12}$ and $C_{24}$), it is observed that their electronic properties can be modified by heteroatom doping. B- and C- atoms which can stimulate hole acceptor or donor states within the Fermi level [12,13] consequently enhance the electronic and conducting properties of $B_{12}N_{12}$ and $C_{24}$ nanocage. Additionally, the drug molecule interacts with C-doped $B_{12}N_{12}$ and B-doped $C_{24}$ nanocages with high sensitivity. Hosseinian et al. [14]
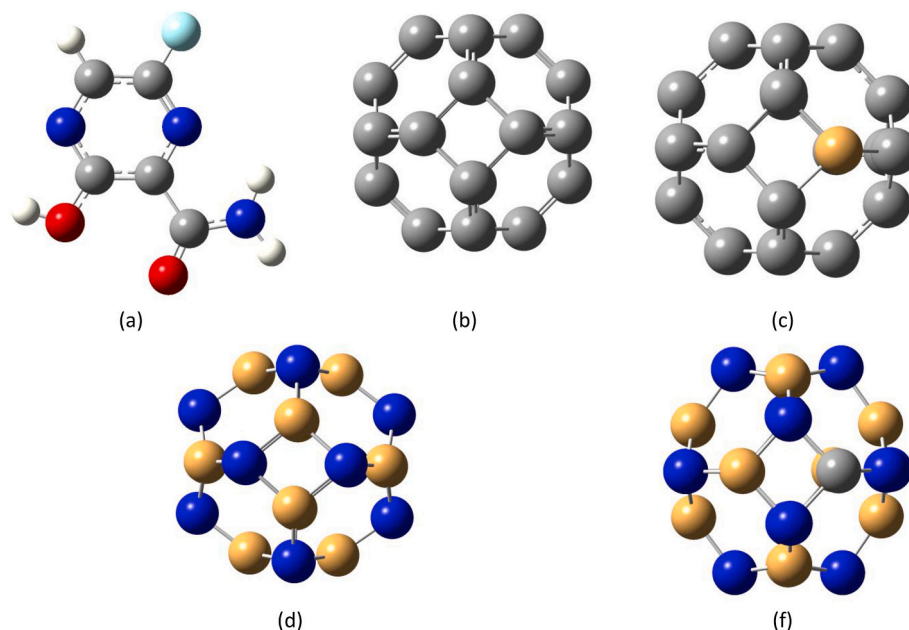
**Fig. 1.** Optimized structure for (a) T-705, (b) $C_{24}$, (c) $C_{23}B$ and (d) $B_{12}N_{12}$ (f) $CB_{11}N_{12}$ nanocages .

investigated the interaction between $C_{24}$ and a widely used molecule for treating cancer – 5-fluorouracil (5-FU). Hazrati and Hadipour [15] investigated how modifications of fullerene $C_{60}$ doped with B, Si and Al atoms influence the adsorption of 5-FU. Comprehensive reviews have been focused on boron-nitride (BN) fullerene-like materials since they have excellent properties [16–19]. A comprehensive experimental and theoretical study on BN nanomaterials for the adsorption of pharmaceutical drugs were performed to examine the synthesis and characterization of BN nanosheets and their applicability for the adsorption of pharmaceutical drugs [20].

The electronic and structural properties of 5-ALA functioned with $B_{12}N_{12}$ and $B_{16}N_{16}$ nanoclusters to further understand $B_{12}N_{12}$ and $B_{16}N_{16}$ capacity for use in drug delivery applications [21]. Interactions between fullerene $C_{24}$ as a potential carrier of ephedrine drug have been studied in detail by a combination of density functional theory (DFT), time dependent DFT (TD-DFT) calculations [22–24]. Parlak et al. [25] examined the interaction of favipiravir on undoped and Si-doped fullerene ($C_{60}$) and the results indicated that Si-doped fullerene are sensitive to the favipiravir molecule. Also, a recent study was conducted by Rad et al. [26] to analyze drug adsorption of favipiravir on first-row transition metals doped with fullerenes ($C_{20}$) and the results showed that Fe, Cr, and Ni-doped fullerene would be potential drug delivery for COVID-19 treatment. Consequently, the objective of the present study is to investigate and compare theoretically the interaction of Favipiravir functionalized at perfect ($B_{12}N_{12}$ and $C_{24}$) and doped ($BC_{23}$ and $CB_{11}N_{12}$) nanocages to provide a useful guidance for the design and improvement of fullerene and boron nitride nanocages capacity for use in drug delivery applications.

## 2. Computational details

The quantum chemical calculations of structure optimizations, electronic structure, and adsorption properties of complexes that consist of Favipiravir drugs at the surface of un-doped $C_{24}$, $B_{12}N_{12}$, boron-doped $C_{24}$ ($BC_{23}$), and carbon-doped $B_{12}N_{12}$ ($CB_{11}N_{12}$) nanocages were performed in gaseous and aqueous phase using the density functional theory (DFT) method with Becke-3-Parameter-Lee-Yang-Parr (B3LYP) and 6-31 g(d,p) basis set to examine of Favipiravir as antiviral for treatment of COVID-19. The aqueous phase was calculated using the self-consistency reaction field (SCRF) approach based on the conductor-

like polarizable continuum model (CPCM) [27].

The adsorption energy ($E_{ads}$) for the full optimization of the Favipiravir (T-705) at the $C_{24}$, $BC_{23}$, $B_{12}N_{12}$ and $CB_{11}N_{12}$ nanocages was calculated by:

$$E_{ads} = E(cage + T - 705) - E(cage) - E(T - 705) \qquad (1)$$

where E(cage + T-705) is the energy of Favipiravir molecule@nanocage, Ecage is the total energy of nanocages, and E(T-705) is the total energy of the Favipiravir molecule.

The quantum molecular descriptors [28,29] of the optimized compounds for instance $E_{HOMO}$, $E_{LUMO}$, energy gap between HOMO and LUMO, dipole moment and natural charges [30,31], ionization potential ($I = -E_{HOMO}$), electron affinity ($A = -E_{LUMO}$), electronegativity $\left( \chi = \frac{I+A}{2} \right)$, global hardness ($\eta = \frac{I-A}{2}$), electronic chemical potential ($\mu = -\left( \frac{I+A}{2} \right)$), electrophilicity ($\omega = \frac{\mu^2}{\eta}$) [32], chemical softness ($\sigma = \frac{1}{2\eta}$) were determined. The present proposals are to investigate the therapeutic potential of $C_{24}$, $BC_{23}$, $B_{12}N_{12}$, and $CB_{11}N_{12}$ nanocage as a drug-delivery system for Favipiravir for treatment of COVID-19 and to explore the efficiency of nanostructure as a drug-delivery system. The principle aspects such as interaction mechanism between Favipiravir drug and $C_{24}$, $B_{12}N_{12}$, $BC_{23}$, and $CB_{11}N_{12}$ nanocages using DFT and TD-DFT calculations have been exhausted to further understand nanocages capacity that has attracted tremendous attention as a most promising drug delivery nanomaterial.

To comparatively analyze the interaction properties of Favipiravir drug based on BN and $C_{24}$ nanocages, the bonding characteristics, adsorption ability, charge transfer, dipole moment, frontier orbitals, energy gaps, molecular electrostatic potential (MEP), partial density of states (PDOS), natural bond orbital (NBO), changes in Gibbs free energy of these complexes have been examined. The time-dependent density functional calculations (TD-B3LYP and TD-CAM-B3LYP) were used to simulate UV and infrared spectroscopy and to exhibit whether the interaction between $B_{12}N_{12}$ and $C_{24}$ nanocages and Favipiravir produces some significant changes in the UV spectrum and vibrational frequencies during the detection of Favipiravir. The effect of long-range corrections has been carried out using the TD-CAM-B3LYP methods [33]. TD-CAMB3LYP methods [34] are used to provide a relatively accurate description of the energies of spectral bands, when there is a significant
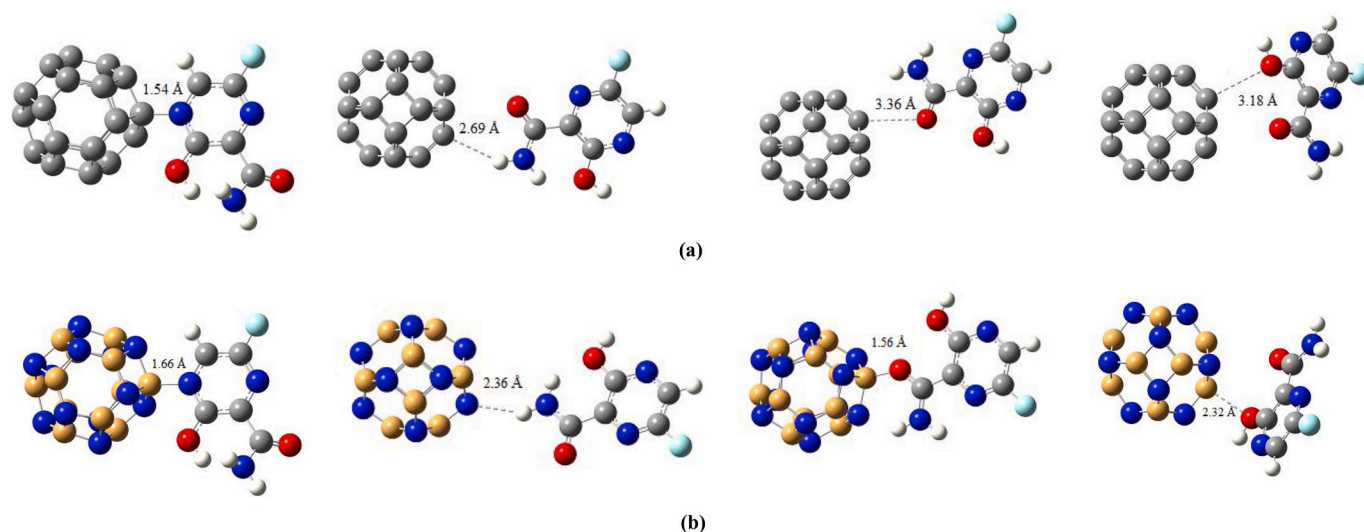
**Fig. 2.** Optimized geometries of the possible interactions between the T-705 drug with (a) $C_{24}$, and (b) $B_{12}N_{12}$ nanocarrier calculated at B3LYP/6-31G(d,p) level of theory.
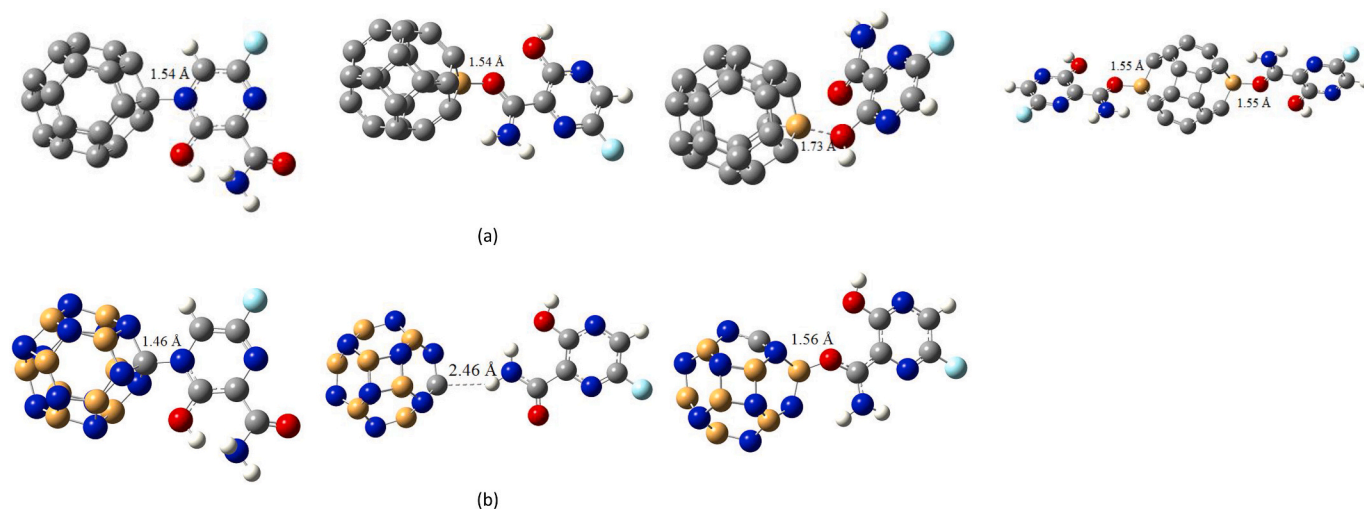


**Fig. 3.** Optimized geometries of the possible interactions between the T-705 drug with functionalized (a) $BC_{23}$, and (b) $CB_{11}N_{12}$ carrier calculated at the B3LYP/6-31G(d,p) level of theory.

charge transfer character in the excited states [35]. K. Petrushenko et al. [36] suggested that the Coulomb-attenuated CAM-B3LYP functional containing 19% short-range exact orbital exchange and 65% long-range exact orbital exchange improves sufficiently the description of CT transitions in comparison with the B3LYP hybrid functional, involving a fixed amount (20%) of exact exchange. Therefore, the TD-CAMB3LYP method can be used for the interpretation of experimental data of the close-lying LE and CT transitions. The thermodynamic parameters such as enthalpy change ($\Delta H$), entropy change ($\Delta S$), and Gibbs free energy ($\Delta G$) were examined in the gas and aqueous phases for T-705@nanocages at 310.15 K (human body temperature) and 298.15 K (storage room temperature). These properties are elucidated using the Gaussian 09 [37]. The GaussSum program was used for PDOS of these systems [38].

**Table 1**
Total energies of T-705/nanocages.

| System | HF(Hartree) |
|---|---|
| $C_{24}$ + Drug(N) | −1521.28179258 |
| $C_{24}$ + Drug(NH2) | −1521.29976973 |
| $C_{24}$ + Drug(O) | −1521.30338089 |
| $C_{24}$ + Drug(OH) | −1521.30280260 |
| $B_{12}N_{12}$ + Drug(N) | −1563.66433686 |
| $B_{12}N_{12}$ + Drug(NH2) | −1563.64235103 |
| $B_{12}N_{12}$ + Drug(O) | −1563.68383936 |
| $B_{12}N_{12}$ + Drug(OH) | −1563.65185512 |
| $C_{23}B$ + Drug(N) | −1508.11200329 |
| $C_{23}B$ + Drug(O) | −1508.12600456 |
| $C_{23}B$ + Drug(OH) | −1508.08755113 |
| $CB_{11}N_{12}$ + Drug(N) | −1576.75954799 |
| $CB_{11}N_{12}$ + Drug(NH2) | −1576.73889024 |
| $CB_{11}N_{12}$ + Drug(O) | −1576.76616441 |

**Table 2**
Geometrical parameters (Å), adsorption energy (eV), and the angle H–N–H of T-705 molecules in the gas and aqeous phase. The values in brackets for double loaded T-705 on $BC_{23}$ nanocage.

| Structure | Gas phase | | | Aqueous phase | | |
|---|---|---|---|---|---|---|
| | $E_b$ | $d_{T-705/cage}$ | ∠H-N-H | $E_b$ | $d_{T-705/cage}$ | ∠H-N-H |
| $T-705/C_{24}$ | −0.085 | 3.355 | 121.319 121.253[a] | −0.055 | 3.526 | 120.511 120.303[a] |
| $T-705/C_{23}B$ | −1.434 (−1.10) | 1.539 (1.55) | 123.179 | −0.947 | 1.519 | 121.579 |
| $T-705/B_{12}N_{12}$ | −1.120 | 1.557 | 124.989 | −1.218 | 1.527 | 122.994 |
| $T-705/CB_{11}N_{12}$ | −1.128 | 1.555 | 125.397 | −1.208 | 1.525 | 123.193 |

[a] Isolated T-705.

## 3. Results and discussion

### 3.1. The interaction of Favipiravir with functionalized $C_{24}$ and $B_{12}N_{12}$ nanocages

#### 3.1.1. Structural analysis

Initially, to identify the most favorable adsorption configurations, geometrically optimization of an individual T-705 at $C_{24}$, $BC_{23}$, $B_{12}N_{12}$, and $CB_{11}N_{12}$ cages were carried out within the gas phase; Figs. 1–3, T-705 was originally located in different orientations around the nanocages surface.

As given in Table 1, it is observed that the adsorption of the drug from O atom (C=O) on the nanocage surface is a more convenient configuration. The optimized geometries of perfect ($C_{24}$, $B_{12}N_{12}$) and functionalized nanocages ($BC_{23}$, $CB_{11}N_{12}$) in the presence of adsorbed T-705 does not affect the planarity of the nanocage. The calculated adsorption energies of the T-705 molecule over $C_{24}$, $BC_{23}$, $B_{12}N_{12}$, and $CB_{11}N_{12}$ cages are about (−0.085, −1.434, −1.120, and −1.128 eV) with corresponding binding distances of 3.355, 1.539, 1.557 and 1.555 Å, respectively. Also, the double T-705 molecules were loaded on $BC_{23}$ nanocage that is more powerful than undoped nanocages, the calculated adsorption energy −1.10 eV. As seen in Table 2. According to the provided results, the T-705 molecule is physisorbed (−0.085 eV) toward $C_{24}$. Compared to perfect $B_{12}N_{12}$ nanocage, the functionalized $B_{12}N_{12}$ ($CB_{11}N_{12}$) nanocage has a slightly higher adsorption energy than its counterpart in $B_{12}N_{12}$. However, for $C_{24}$ and $BC_{23}$, the binding energy in the gas phase is greater than the aqueous phase, for $B_{12}N_{12}$, $CB_{11}N_{12}$

binding energy is enhanced in the solvent phase. Hence, the solubility of the $T-705/B_{12}N_{12}$ and $T-705/CB_{11}N_{12}$ increases in the solvent phase with regard to the gas phase, indicating the electrostatic bond in the interaction process.

The average C—C and B—N bond lengths in $C_{24}$ and $B_{12}N_{12}$ nanocage are 1.492 and 1.486 Å, respectively, which is consistent with the reported values [39]. The experimental and theoretical geometrical parameters of T-705 molecule are presented in Table 3 [5,6]. Upon the interaction of T-705 molecule, the bond lengths of B—N for the $B_{12}N_{12}$ and $CB_{11}N_{12}$ cages clusters were found to be 1.576 and 1.554 Å. As a result, the bond length of nanocages is elongated due to the adsorption of T-705 at the nanocages. Moreover, the bond length N—H and angle H–N–H of the adsorbed T-705 molecule on the $BC_{23}$, $B_{12}N_{12}$ and $CB_{11}N_{12}$ cages, are higher than the isolated T-705 bond length (N–H = 1.007 Å) and ∠H–N–H 121.3° (Table 2).

The interaction between nanocages and pharmaceutical molecules affects the electronic properties, implying that the electronic properties of the $BC_{23}$, $B_{12}N_{12}$, and $CB_{11}N_{12}$ nanocages are very sensitive to the T-705 adsorption in comparison with the pure $C_{24}$ nanocage. Indeed, to understand the structure and reactivity of T-705, $C_{24}$, $BC_{23}$, $B_{12}N_{12}$, and $CB_{11}N_{12}$ and their complexes. The global softness (σ), chemical potential (μ), global hardness (η), and the electrophilicity index (ω) are presented in Table 4. According to the provided results, the energy gap and η of $B_{12}N_{12}$ nanocage equal to 6.84 eV and 3.422 eV respectively which in agreement with [40]. From Table 4, the energy gap and η values pointed that T-705@doped nanocages are more reactive than T705@perfect nanocages. As compared to the perfect $C_{24}$ and $B_{12}N_{12}$ nanocage, B doped $C_{24}$ ($BC_{23}$) and C doped $B_{12}N_{12}$ ($CB_{11}N_{12}$) nanocage, are more reactive as indicated from the energy gap and η values.

Upon the interaction of T-705 over nanocages, the energy gap reduces except T-705@$BC_{23}$ in the aqueous phase, indicating the improvement in reactivity. As seen in Table 4, the μ and ω value increases with the adsorption of T-705 on doped $CB_{11}N_{12}$ nanocage, implying the increase in reactivity and electrophilicity of the complex. Consequently, $BC_{23}$ and $CB_{11}N_{12}$ are more powerful toward electron-rich or attracting nucleophiles moieties. In contrast, the adsorption of the T-705 molecule with the $C_{24}$ surface has less effect on the electronic properties of $C_{24}$ due to the lowest binding energy.

The global electrophilicity index [41] measures the stability of energy when an electronic charge is acquired from the surrounding medium. Two descriptors can be used to explain the ability of a chemical species to donate or accept an electron. Eqs. (2) and (3) are used to calculate the electron donor capability ($\omega^-$), electron acceptor capability

**Table 3**
Structural parameters of T-705 in the gas phase.

| Bond length (Å) | Experimental [6] | B3LYP | Bond angle (°) | Experimental [6] | B3LYP | Dihedral angle (°) | Experimental [6] | B3LYP |
|---|---|---|---|---|---|---|---|---|
| C1-C4 | 1.390 | 1.394 | C2-O14-H15 | 109.5 | 106.0 | N8-C6-C3-N11 | −0.4 | −0.02821 |
| C1-N12 | 1.306 | 1.331 | O14-C2-N12 | 115.6 | 117.0 | N8-C6-C3-C2 | 178.9 | 179.97212 |
| C1-H5 | 0.930 | 1.086 | O14-C2-C3 | 123.5 | 121.7 | N11-C3-C2-N12 | 0.2 | 0.01715 |
| C2-N12 | 1.306 | 1.338 | C2-C3-C6 | 120.7 | 123.6 | N11-C4-C1-N12 | 0.6 | 0.02034 |
| C2-O14 | 1.328 | 1.338 | O7-C6-C3 | 119.7 | 122.6 | C3-C2-N12-C1 | 0.3 | −0.00888 |
| C2-C3 | 1.397 | 1.417 | C7-C6-N8 | 123.1 | 124.0 | C3-N11-C4-C1 | −0.9 | −0.01187 |
| C3-C6 | 1.481 | 1.511 | C6-N8-H9 | 120.7 | 118.0 | O7-C6-C3-C2 | −1.0 | −0.00135 |
| C3-N11 | 1.335 | 1.341 | C6-N8-H10 | 120.7 | 120.7 | O7-C6-C3-N2 | 179.1 | 179.99833 |
| C4-F13 | 1.339 | 1.340 | C6-C3-N11 | 121.4 | 117.2 | O14-C2-N12-C1 | 179.7 | 179.98897 |
| C4-N11 | 1.295 | 1.312 | C3-N11-C4 | 116.3 | 118.6 | F13- C4-C1-N12 | 179.2 | 179.98897 |
| C6-O7 | 1.244 | 1.223 | N11-C4-F13 | 116.8 | 117.6 | F13- C4-N11-C3 | 0.4 | 0.01907 |
| C6-N8 | 1.318 | 1.361 | N11-C4-C1 | 123.3 | 122.7 | O14- C2-C3-C6 | −1.0 | −0.00902 |
| N8-H9 | 0.860 | 1.007 | F13-C4-C1 | 119.9 | 119.7 | C2 –N12-C1-C4 | −0.9 | −0.01187 |
| N8-H10 | 0.860 | 1.008 | N12-C1-H5 | 119.4 | 118.6 | C1-C4-N11-C3 | −0.7 | −0.00632 |
| O14-H15 | 0.820 | 0.972 | C1-N12-C2 | 117.0 | 118.5 | | | |
| | | | O14-C2-N12 | 115.6 | 117.0 | | | |
| | | | H9-N8-H10 | 120.0 | 121.3 | | | |
| | | | C4-C1-H5 | 119.4 | 121.6 | | | |
| | | | N12-C2-C3 | 120.8 | 121.2 | | | |
| | | | C3-C6-O7 | 119.7 | 122.6 | | | |
| | | | N8-C6-C3 | 117.3 | 123.6 | | | |

**Table 4**
Frontier molecular orbital energies, HOMO–LUMO energy gap, global hardness (η), chemical potential (μ), global electrophilicity (ω), electron donor capability (ω⁻), electron acceptor capability (ω⁺) and global softness (σ⁻¹) values of the T-705 molecule, perfect (C₂₄, B₁₂N₁₂) and functionalized (BC₂₃, CB₁₁N₁₂) nanocages and their complexes with T-705 drug.

| Structure | Gas phase | | | | | | | | | Aqueous phase | | | | | | | | |
|---|---|---|---|---|---|---|---|---|---|---|---|---|---|---|---|---|---|---|
| | $E_{HOMO}$ (eV) | $E_{LUMO}$ (eV) | $\Delta E$ (eV) | $\mu$ (eV) | $\eta$ (eV) | $\omega$ (eV) | $\omega^-$ (eV) | $\omega^+$ (eV) | $\sigma^{-1}$ (eV) | $E_{HOMO}$ (eV) | $E_{LUMO}$ (eV) | $\Delta E$ (eV) | $\mu$ (eV) | $\eta$ (eV) | $\omega$ (eV) | $\omega^-$ (eV) | $\omega^+$ (eV) | $\sigma^{-1}$ (eV) |
| T-705 | −6.82 | −2.22 | 4.60 | −4.52 | 2.3 | 4.441 | 6.988 | 2.469 | 0.217 | −6.915 | −2.183 | 4.731 | −4.549 | 2.366 | 4.373 | 6.943 | 2.394 | 0.211 |
| C24 | −5.870 | −3.356 | 2.513 | −4.613 | 1.257 | 8.446 | 10.930 | 6.317 | 0.398 | −5.789 | −3.276 | 2.513 | −4.532 | 1.256 | 8.174 | 10.598 | 6.065 | 0.398 |
| C23B | −5.82 | −3.13 | 2.683 | −4.475 | 1.345 | 7.444 | 9.850 | 5.375 | 0.372 | −5.738 | −3.055 | 2.683 | −4.396 | 1.342 | 7.203 | 9.568 | 5.172 | 0.373 |
| B12N12 | −7.70 | −0.86 | 6.841 | −4.282 | 3.422 | 2.678 | 5.246 | 0.966 | 0.146 | −7.698 | −0.805 | 6.892 | −4.252 | 3.446 | 2.623 | 5.179 | 0.928 | 0.146 |
| CB11N12 | −5.49 | −0.96 | 4.533 | −3.225 | 2.265 | 2.296 | 4.192 | 0.966 | 0.221 | −7.742 | −5.490 | 2.252 | −6.616 | 1.126 | 19.438 | 22.887 | 16.271 | 0.444 |
| T-705/C24 | −5.70 | −3.192 | 2.508 | −4.445 | 1.254 | 7.881 | 10.261 | 5.815 | 0.399 | −5.801 | −3.303 | 2.498 | −4.552 | 1.249 | 8.294 | 10.727 | 6.174 | 0.400 |
| T-705/C23B | −5.079 | −2.833 | 2.247 | −3.956 | 1.124 | 6.966 | 15.261 | 11.176 | 0.445 | −5.738 | −3.055 | 2.683 | −4.396 | 1.342 | 7.203 | 9.085 | 5.128 | 0.373 |
| T-705/B12N12 | −6.57 | −3.38 | 3.194 | −4.975 | 1.595 | 7.759 | 10.446 | 5.471 | 0.313 | −6.974 | −2.819 | 4.154 | −4.897 | 2.078 | 5.772 | 8.479 | 3.583 | 0.241 |
| T-705/CB11N12 | −4.510 | −3.374 | 1.137 | −3.942 | 0.568 | 13.668 | 15.710 | 11.768 | 0.879 | −4.809 | −2.829 | 1.979 | −3.819 | 0.989 | 7.368 | 9.402 | 5.583 | 0.505 |

(ω⁺) values [40], respectively.

$$\omega^- = \frac{(3I+A)^2}{16(I-A)} \qquad (2)$$

$$\omega^+ = \frac{(I+3A)^2}{16(I-A)} \qquad (3)$$

The electron-donating capability (ω⁻) value of T-705 was observed to be greater than its electron-accepting (ω⁺) capability as well as the electron-accepting (ω⁺) capability values of nanocages are greater than T-705 molecule. The aforementioned results show that the T-705 molecule has good kinetic stability and electron-donating ability.

### 3.2. Frontier molecular orbital analysis

The eigenvalue of the Frontier molecular orbitals (HOMO and LUMO) and $\Delta E_{HOMO-LUMO}$ energy gap for these complexes play a significant role in controlling many chemical activity, electrical, and optical properties [42,43]. They are responsible for properties of charge transfer, the energies of HOMO and LUMO values indicate the ability of a system to donate and accept an electron. The aforementioned results show that the doping atoms reduce the energy gap of the nanocarriers. As seen in Table 4 the energy gap of the complex is much lower than those of isolated nanocages and T-705. Concerning the Favipiravir molecule, the energy gap of 4.6 eV that is consistent with [5].

### 3.3. Molecular electrostatic potential (MEP) analysis

Molecular electrostatic potential (MEP) analysis explored the reactivity and the interaction mechanism between T-705 and B₁₂N₁₂, CB₁₁N₁₂, C₂₄, BC₂₃ nanocages. MEP plots are used for predicting nucleophilic and electrophilic attacks and hydrogen bonding interaction [44]. Electrophilic reactivity was associated with the negative (red color) of MEP with the high electron density and the positive regions (blue color) with the low electron density. As demonstrated in these configurations, the positive charges over the T-705 were illustrated by the blue colors in the adsorption process that acts as an electron donor (Fig. 4). Whereas the negative charges over the B₁₂N₁₂, CB₁₁N₁₂, C₂₄, BC₂₃ nanocages are represented by the red colors that acts as an electron acceptor. Hydrogen atoms of OH group of drug molecules have the lowest electron density with blue color (electropositive atom), consequently it can be considered as the acidic hydrogen atom, the electrons around the B·O bond are depleted and accumulated on O atom with a small charge of about 0.08e transfer from the gas molecule to the surface.

### 3.4. Thermodynamic parameters and nature of the binding forces

The thermodynamic parameters such as enthalpy change (ΔH), entropy change (ΔS), and Gibbs free energy (ΔG) were evaluated in the gas and aqueous phases for T-705@nanocages at 310.15 K (human body temperature) and 298.15 K (storage room temperature). The values of ΔG, ΔH, and ΔS are collected in Table 6. The adsorption of drug molecules is an exothermic process.. As seen in Table 5 that the positive ΔG value of T-705@C24 indicated that the reactions are non-spontaneous that not favorable adsorption at ambient conditions in agreement with [45]. In contrast, the thermodynamic parameters imply that the adsorption of T-705 @ B₁₂N₁₂, T-705 CB₁₁N₁₂, and T-705 BC₂₃ complexes is strongly favorable due to the spontaneously adsorption of drug on the host nanocage surface. Comparison results of thermodynamic parameters demonstrate that the adsorption of T-705 on functionalized (CB₁₁N₁₂, and BC₂₃) nanocage are more favorable than the pristine model (B₁₂N₁₂ and C₂₄) surfaces.

To examine the effect of solvent on the interaction of T-705 drug at the pristine surface, C-doped B₁₂N₁₂ and B-doped C₂₄ nanocages, the
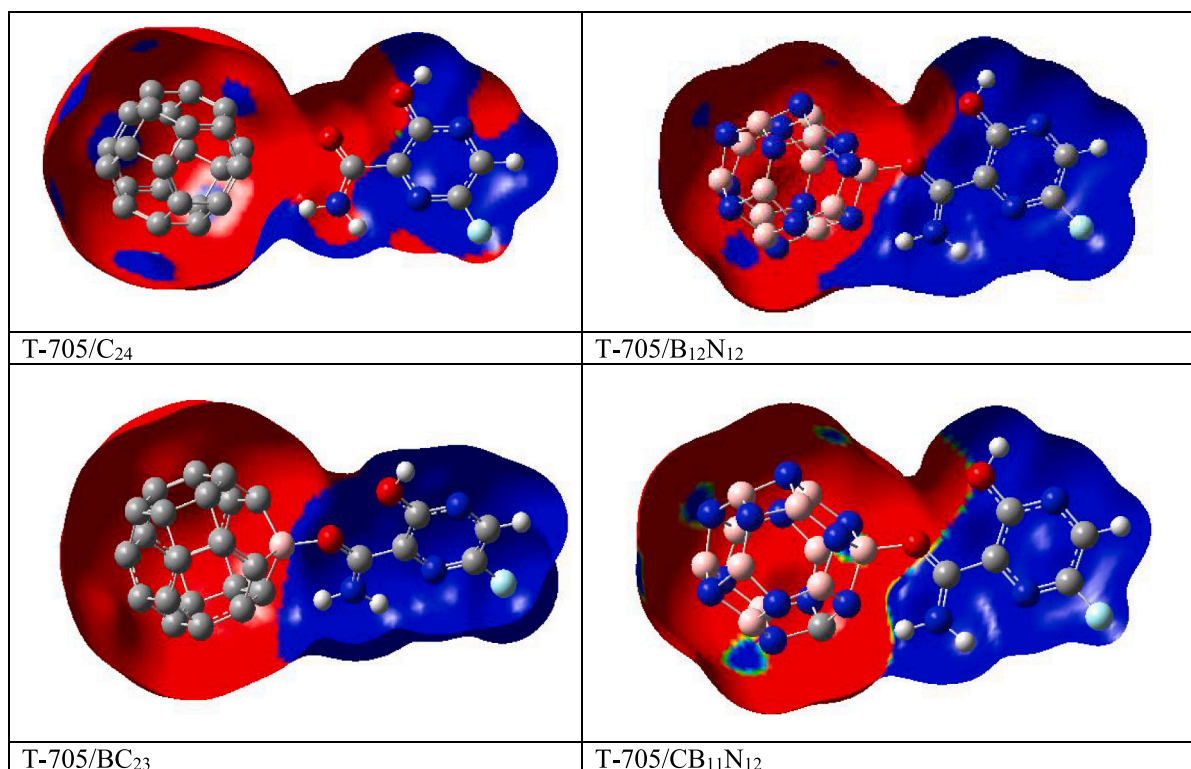
**Fig. 4.** ESP of the most stable T-705 @ nanocages.

**Table 5**
Thermodynamic parameters (Kcal/mol) of T-705/$C_{24}$, T-705/$C_{23}B$, T-705/$B_{12}N_{12}$ and T-705/$CB_{11}N_{12}$ complexes in gas and aqueous phases at $T$ = 298.15 and 310.15 K.

| Structure | 298.15 | | | | | | 310.15 | | | | | |
|---|---|---|---|---|---|---|---|---|---|---|---|---|
| | Gas phase | | | Aqueous phase | | | Gas phase | | | Aqueous phase | | |
| | $\Delta G$ | $\Delta S$ | $\Delta H$ | $\Delta G$ | $\Delta S$ | $\Delta H$ | $\Delta G$ | $\Delta S$ | $\Delta H$ | $\Delta G$ | $\Delta S$ | $\Delta H$ |
| T-705/$C_{24}$ | 7.472 | −27.948 | −1.048 | 8.256 | −27.487 | 0.066 | 7.612 | −26.348 | −0.562 | 8.586 | −27.343 | 0.109 |
| T-705/$C_{23}B$ | −19.805 | −41.235 | −30.666 | −19.427 | −49.797 | −34.266 | −8.303 | −44.096 | −21.972 | −18.829 | −49.79 | −34.264 |
| T-705/$B_{12}N_{12}$ | −10.897 | −45.233 | −24.467 | −13.384 | −44.155 | −26.542 | −10.445 | −45.173 | −24.448 | −12.854 | −44.079 | −26.519 |
| T-705/$CB_{11}N_{12}$ | −11.237 | −45.065 | −24.858 | −13.552 | −43.362 | −26.475 | −10.890 | −43.533 | −24.391 | −13.033 | −43.28 | −26.449 |

changes of $\Delta G$ in the water as an important solvent in the biological system are calculated. According to the provided results in Table 5, all the thermodynamic functions of $C_{24}$ and $BC_{23}$ in the gas phase are higher than those in the aqueous phase, whereas for $B_{12}N_{12}$ and $CB_{11}N_{12}$ they are higher in the aqueous phase than gas phase. This can be explained due to the molecular polarities of $B_{12}N_{12}$ and $CB_{11}N_{12}$ in the gas phase are lower than in the aqueous phase, which in turn increased the thermodynamic parameters to some extent. Furthermore, compared to the $\Delta H$ values, the calculated $\Delta G$ values are less negative, implies an entropy reduction associated with the examined complexes. The negative value of $\Delta S$ indicates that the interaction that takes place between T-705 drug and $B_{12}N_{12}$, $CB_{11}N_{12}$, and $BC_{23}$ nanocage $\Delta H < 0$, $\Delta S < 0$ is corresponding to the van der Waals interaction and hydrogen bond formation, this is agreement with [46]. The thermodynamic parameters and adsorption calculations indicate that $B_{12}N_{12}$ and the functionalized $CB_{11}N_{12}$, $BC_{23}$ nanocage can be a good promising candidate for delivery of T-705 drug.

### 3.5. Non-covalent interactions

The non-covalent interactions (NCI) are visualization tools that play an essential role in maintaining the 3D structure. The NCI used to

recognize non-covalent interactions involve intermolecular forces within molecules such as van der Waals, hydrogen bonds, and steric clashes based on electron density and gradient electron density (RDG). RDG is defined as

$$\text{RDG(r)} = \frac{1}{2(3\pi^2)^{1/3}} \frac{|\nabla\rho(r)|}{\rho(r)^{4/3}} \tag{4}$$

To examine the non-covalent interactions between the favipiravir drug and the nanocage, as plotted in Figs. 5 and 6 the scatter graphs between the reduced density gradient (RDG) and the electron density ($\rho$). From the graph, sign ($\lambda_2$) $\rho$ decreases for strong interactions such as H-bond are represented by blue color, sign ($\lambda_2$) $\rho$ increases for red colors that represented strong repulsion such as steric effect in cage, while near zero for the van der Waals (vdW) interactions are represented by green color. The vdW interactions are short-range and weak interaction. As seen from Figs. 5 and 6, The non-covalent interactions of T-705 drugs with nanocages are weak interactions which is an advantage for drug release from the nanocage.

### 3.6. The electron localization function

The electron localization function (ELF) is a method used to measure electron localization in atomic and molecular systems [47]. ELF images
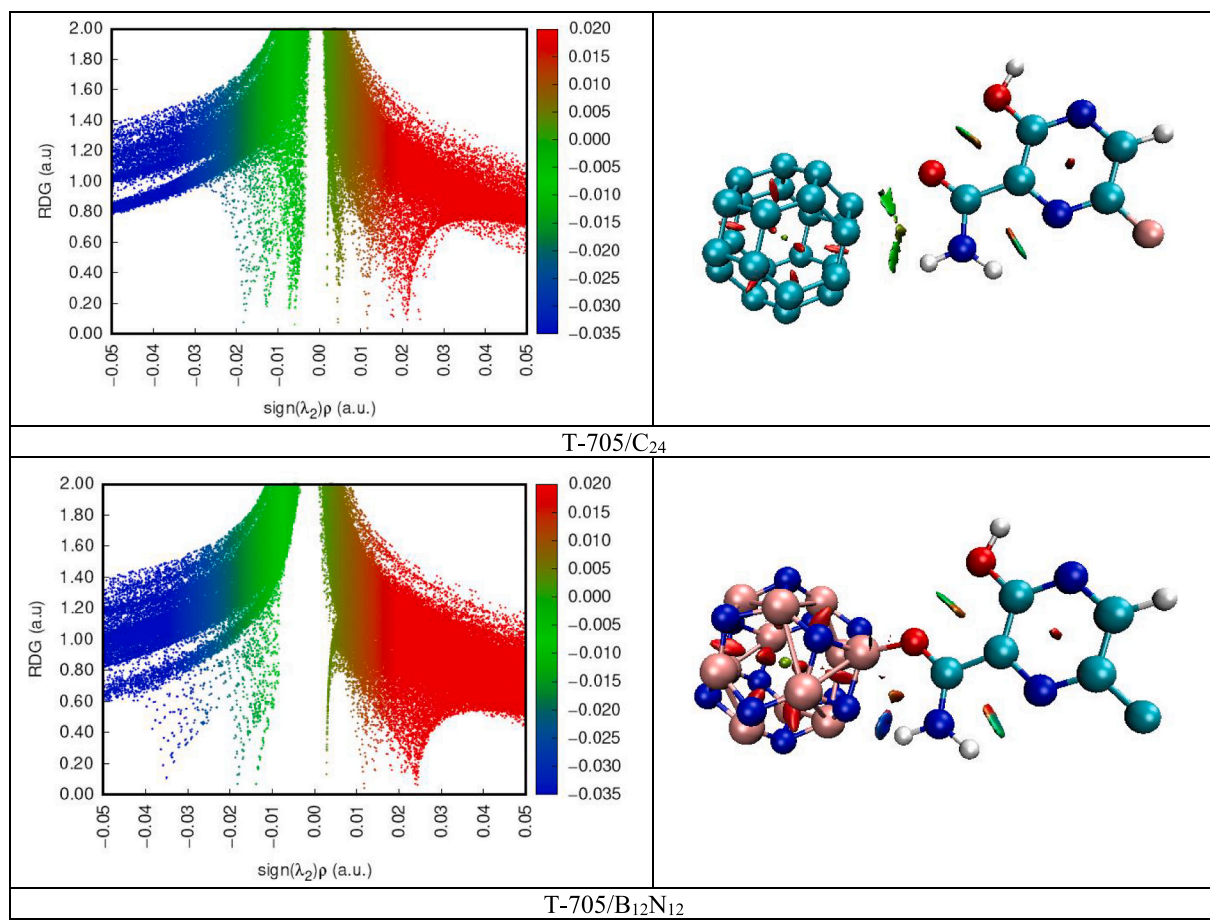
**Fig. 5.** Non-covalent interaction of complex between the drug molecule T-705 and the perfect nanocages.

of nanocages and drug-nanocages are shown in Fig. 6. The values of ELF are in range from 0.0 to 1.0 that value of 0.0 corresponding to zero localization (blue areas) where the value 0.5 and 1.0 corresponding to the electron gas (green areas) and perfect localization(red areas), respectively [48,49]. The electron density of nanocages were changed after the nanocage-drug formation as ELF seen in Figs. 7 and 8.

Images of ELF provide information about transition occurring from nanocages to drug and from drug to nanocages as seen in Table 6 of NBO analysis of the complexes.

### 3.7. Natural bond orbital (NBO) analysis

NBO analysis is effective for identifying inter- and intra-molecular bonding [50,51]. On the basis of the NBO analysis, this bonding–antibonding interaction can be described quantitatively using second-order perturbation interaction energy $E^{(2)}$. From the second-order perturbation approach, the stabilization energy $E^{(2)}$ associated with i (donor) - j (acceptor) delocalization is investigated:

$$E^{(2)} = q_i \frac{F^2(i,j)}{\varepsilon_j - \varepsilon_i} \tag{5}$$

where $q_i$ is the occupancy of donor orbital, $\varepsilon_i$ and $\varepsilon_j$ are orbital energies (diagonal elements) and F(i,j) is the off-diagonal Fock matrix element. The analysis of NBO for these complexes represented that the binding of T-705 drug to the functionalized $C_B$-doped $B_{12}N_{12}$ and B-doped $C_{24}$ nanocage arises essentially from the induced polarization of the T-705 molecule under the electric field created by the doped nanocages. In the most stable configurations, the charges of about 0.323, 0.299, and 0.303 electrons are transferred from the T-705 molecule as an electron donor

to the $BC_{23}$, $B_{12}N_{12}$, and $CB_{11}N_{12}$ (electron acceptor). Therefore, the strongest stabilization of the interaction occurs between effective acceptors and effective donors.

As given in Table 6, for T-705/$C_{24}$ the value of E2 for the intramolecular interactions within T-705 was mainly between $\Pi^*$ (C37-C30) and $\Pi^*$ (C26-O25) is equal 83.07 kcal mol$^{-1}$. It is remarkable to mention that the intermolecular interactions between $C_{24}$ and T-705 was lower with $E^2$ value of 0.99 kcal mol$^{-1}$. The T-705/ $BC_{23}$, T-705/$B_{12}N_{12}$, and T-705/ $CB_{11}N_{12}$ complexes show strong intermolecular between nanocage and drug molecule with $E^2$ values of 153.22, 131.59, and 98.19 kcal mol$^{-1}$. The intermolecular interactions of The T-705/ $BC_{23}$ was mainly between LP (O25) and $\sigma^*$ (B3), for T-705/$B_{12}N_{12}$ was mainly between LP (O25) and $\sigma^*$ (B6), and for T-705/ $CB_{11}N_{12}$ was mainly between LP (O25) and $\sigma^*$ (N17-B6). The stabilization energy of T-705/$BC_{23}$ is greater than those for T-705/ $B_{12}N_{12}$ and T-705/$CB_{11}N_{12}$ complexes due to the stronger hyperconjugative intermolecular interactions. Intramolecular interactions for T-705/$BC_{23}$, T-705/$B_{12}N_{12}$, and T-705/ $CB_{11}N_{12}$ complexes were lower compared with The intermolecular interactions. The intramolecular interaction for T-705/BC23 within BC23 was between $\Pi$ (C5-C6) and LP* (B3) with $E^2$ value 9.53 kcal mol$^{-1}$, for T-705/$B_{12}N_{12}$ within B12N12 was between LP (N20) and $\sigma^*$(B6-O25) with $E^2$ value 12.07, and for T-705/ $CB_{11}N_{12}$ within T-705 was between $\sigma$ (C30-N31) and $\sigma^*$ (C26-O25) with $E^2$ value 0.92 kcal mol$^{-1}$. In terms of the NBO approach, it can be shown that strong intermolecular interactions have mainly contributed to the increased stability in the T-705/ $BC_{23}$, T-705/$B_{12}N_{12}$, and T-705/ $CB_{11}N_{12}$ systems.

### 3.8. The projected density of states (PDOS) analysis

The projected density of states (PDOS) of T-705 adsorbed at $C_{24}$, $BC_{23}$, $B_{12}N_{12}$, and $CB_{11}N_{12}$ in gas and aqueous media as a real living
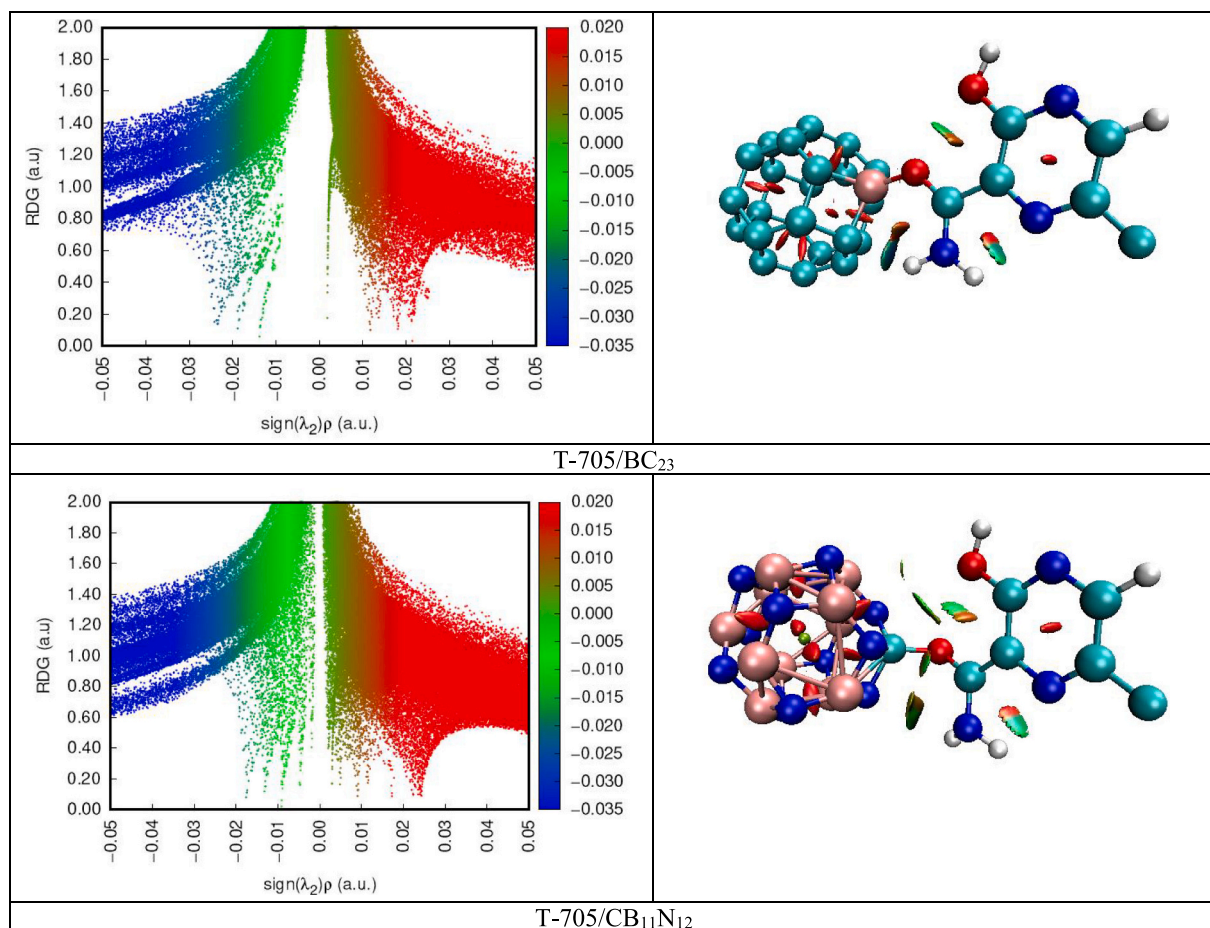
**Fig. 6.** Non-covalent interaction of complex between the drug molecule T-705 and the doped nanocages.

environment has been explained to analyze the interactions between the T-705 drug and the $C_{24}$, BC23, $B_{12}N_{12}$ and $CB_{11}N_{12}$ sites. The PDOS of the T-705 at $BC_{23}$, $B_{12}N_{12}$, and $CB_{11}N_{12}$ complexes in different forms was significantly affected owing to the interaction with various nanocages. The PDOS of the studied complex show lowering in the energy gap as compared to isolated nanocages due to the formation of a new peak in the region of the band gap. The band gap of nanocage $BC_{23}$, $B_{12}N_{12}$ and $CB_{11}N_{12}$ are 2.683, 6.841, 4.533 eV, while the band gap of the T-705 adsorbed at BC23, $B_{12}N_{12}$ and $CB_{11}N_{12}$ complexes are 2.247, 3.194, 1.137 eV. As observed in Figs. 9 and 10, the calculated PDOS of C-2p, B-2p, O-2p orbitals on $B_{12}N_{12}$, $CB_{11}N_{12}$, and $BC_{23}$ appear stronger hybridization than $C_{24}$ due to 2p states distribution from −7.3 to −16.8 eV below the Fermi level.

Also, the intensity of carbon and boron states of T-705@$BC_{23}$ and T-705@$CB_{11}N_{12}$ above the Fermi level reduces when compared with boron and carbon states without T-705 as shown in Figs. 9 and 10, meaning that O-2p orbitals of T-705 not interact only with C-π orbitals but also with C-π* orbitals that doped at BN nanocage. The oxygen atom of C=O (T-705) form essentially a planar structure with c-doped and B-doped atoms (functionalized nanocages) which means $sp^2$ orbital hybridization. It is worth noting that the PDOS of C atoms show stronger intensity near the Fermi level, indicating the $BC_{23}$ is more active than the $CB_{11}N_{12}$, corresponds to the binding energies listed in Tables 2 and 6. The interaction of T-705 with the BC23, $B_{12}N_{12}$ and $CB_{11}N_{12}$, the overlap between the B atom states ($BC_{23}$) and the states of oxygen atom (C=O T-705) spread over from −6.4 eV to −16.8 eV as seen in Figs. 9 and 10. Moreover, a significant overlap of C atom ($CB_{11}N_{12}$) with oxygen atom of C=O (T-705) between −7.6 eV and −17.3 eV has been observed. Additionally, the PDOS of T-705 at the $C_{24}$ and $CB_{11}N_{12}$ in

water solvent, no band appear in the region of the band gap and this is due to the inclusion of water molecules in the system. The positions of HOMO and LUMO changed due to inclusion of water molecules and this led to decreasing the band gap value of T-705@$C_{24}$, T-705@BC23 but increasing of T-705@$B_{12}N_{12}$ and T-705@$CB_{11}N_{12}$.

### 3.9. UV–visible analysis

The time-dependent density functional theory (TD-DFT) calculations were investigated with the CAM-B3LYP functional [50] since it gives rise to more reliable results compared to pure B3LYP on the nature of electronic transitions spectra to get further insights into the electronic absorption of T-705–nanocage complexes in the gas and aqueous phases. The theoretical UV–vis parameters of T-705, nanocages, and the T-705–nanocage complexes are summarized in Tables 7 and 8. According to theoretical calculations represented in Table 7, the T-705 shows four strong peaks at 287.37, 208.63, 181.49, and 163.23 nm with energies of 4.314, 5.943, 6.831 and 7.596 eV for the main electron transitions, respectively. The UV spectrum of T-705 has a sharply intense peak in 165.72–289.33 nm in the water phase. The largest contribution to charge transition at 287.4 nm for T-705 was 98% from HOMO to LUMO [51,52]. The pure $CB_{11}N_{12}$ UV spectrum shows two separated peaks of absorption, located at wavelengths of 216.00 and 261.56 nm. It displayed that the maximum absorption at 518.47, 191.45, 272.61 nm for the $BC_{23}$, $B_{12}N_{12}$, $CB_{11}N_{12}$ corresponds to 2.391, 6.476, and 4.548 eV that represent the HOMO to LUMO excitation, and in turn is a charge transfer from the T-705 to nanocage. After the interaction of T-705 and nanocage with the B atom of $B_{12}N_{12}$, B-doped of the $BC_{23}$ and C-doped of, $CB_{11}N_{12}$, the main absorption peaks are shifted to higher
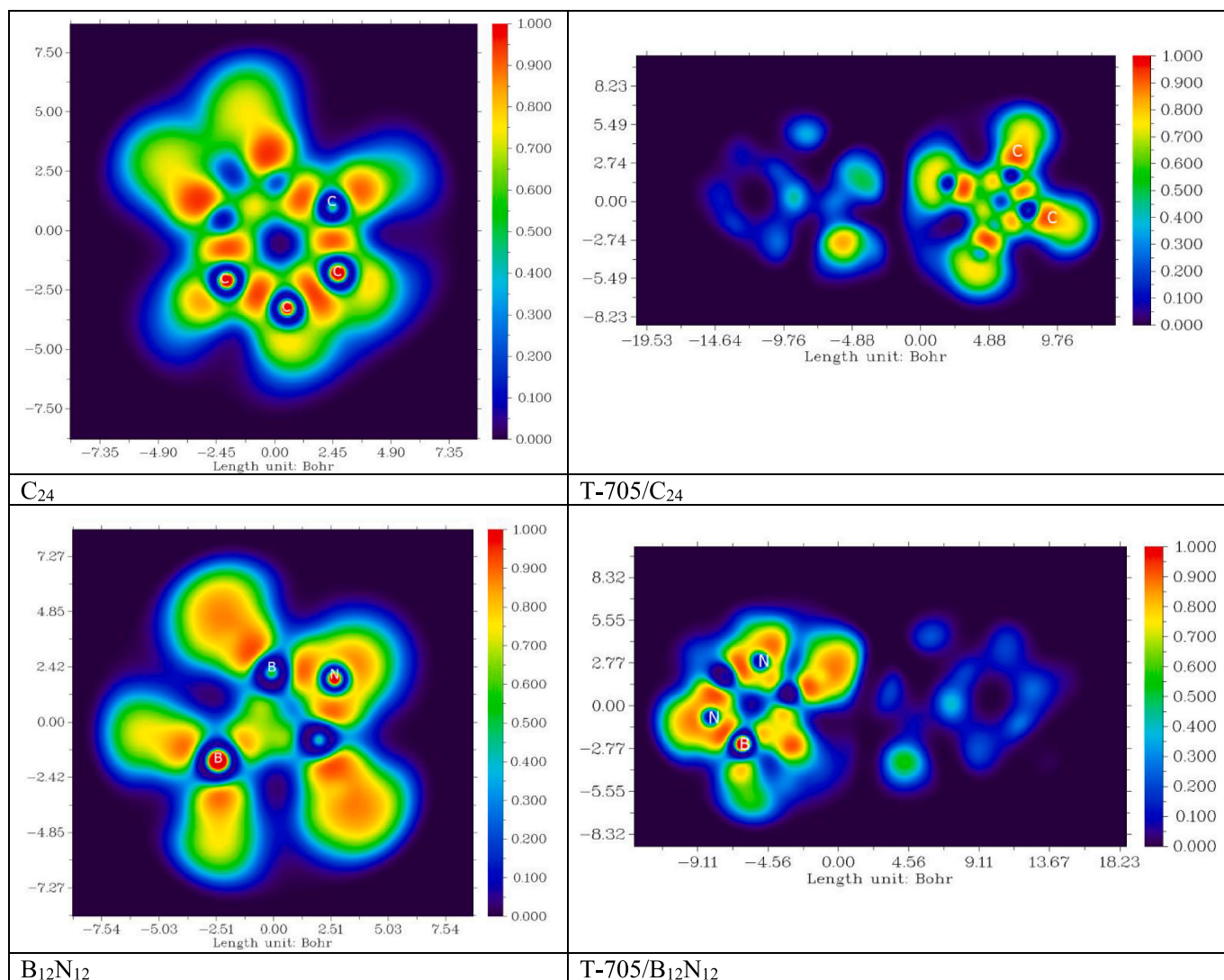
**Fig. 7.** ELF of the perfect nanocages and complexes.

wavelengths ($\lambda_{max}$) at 299.75, 571.96 and 329.38 nm and the adsorption intensity decreased to 4.136, 2.168 and 3.764 eV than isolated T-705 and nanocage.

For the aqueous phase the first absorption peak of the complexes (T-705 at $C_{24}$, $BC_{23}$, and $B_{12}N_{12}$), is located at the wavelength of 381.17, 563.71, and 305.22 nm, which is a shift of 4.96–8.25 nm in comparison with the gas phase, however, the shift of the T-705-$CB_{11}N_{12}$ absorption peak is even more pronounced (22.74 nm). For T-705/$BC_{23}$ complex, the maximum absorption at 571.96 nm is assigned to the transition from the HOMO-2 to the LUMO (55%) molecular orbital in the visible region. This predicted transition is n-π* nature. The HOMO-3 - LUMO (88%) transition (n - π* nature) is assigned to the absorption band of T-705-$CB_{11}N_{12}$ located at 329.2 nm in the calculated spectrum (f = 0.0032). The most significant contribution form T-705@$B_{12}N_{12}$ complex noticed from HOMO-3 - LUMO with 74% of the 0.1837 oscillator strength. Furthermore, it is significant that, when T-705 is adsorbed over the $C_{24}$ nanocage, the wavelength of adsorption is significantly increased to 386.1 nm, which arised from HOMO-3 to LUMO+1 with 56% of the 0.0592 oscillator strength and π-π* transition. In contrast, the CAM-B3LYP method exhibited slight overestimates on the excitation energies of T-705/BC23, T-705/$B_{12}N_{12}$, and T-705/$CB_{11}N_{12}$ complexes and underestimates at T-705/$C_{24}$ as compared to the UB3LYP method in gas and aqueous phases, Tables 9 and 10.

### 3.10. IR spectrum

Vibrational frequencies for the perfect ($B_{12}N_{12}$ and $C_{24}$) and doped ($BC_{23}$ and $CB_{11}N_{12}$) nanocages and their complexes with Favipiravir drug were investigated to evaluate the changes in the bonds stretching vibrational frequency of the Favipiravir before and after the interaction with nanocages. According to Fig. 11, the location of each vibration for doped ($BC_{23}$ and $CB_{11}N_{12}$) differ compared to the pure ($B_{12}N_{12}$ and $C_{24}$) nanocages due to the presence of doped B and C atoms. Literature review revealed that the stretching vibration of B—C is about 1020 cm$^{-1}$ [53], that is in agreement with the calculated values. As expected, the number of vibration peaks for doped ($BC_{23}$ and $CB_{11}N_{12}$) nanocages is greater than those for perfect ($B_{12}N_{12}$ and $C_{24}$) [53]. The most important associated vibration frequencies were strongly examined: $\nu$(C=O) and $\nu$(N—H) bonds of amid functional group and $\nu$(O—H) bond of the Favipiravir molecule were completely in accordance with the Favipiravir molecule in the literature [5]. When Favipiravir get adsorbed on the surface of perfect ($B_{12}N_{12}$ and $C_{24}$) and doped ($BC_{23}$ and $CB_{11}N_{12}$) nanocages, the value of vibrational frequencies as well as IR intensity were altered. Fig. 11 shows that not only the new vibrations bond appeared upon adsorption of this molecule on doped ($BC_{23}$ and $CB_{11}N_{12}$) nanocages, but also some peaks were shifted. For instance, the $\nu$(C=O) of the drug before adsorption (1802 cm$^{-1}$) shifted to the low values (1785, 1716, 1724 and 1723 cm$^{-1}$) depending on the kind of nanocage $C_{24}$,
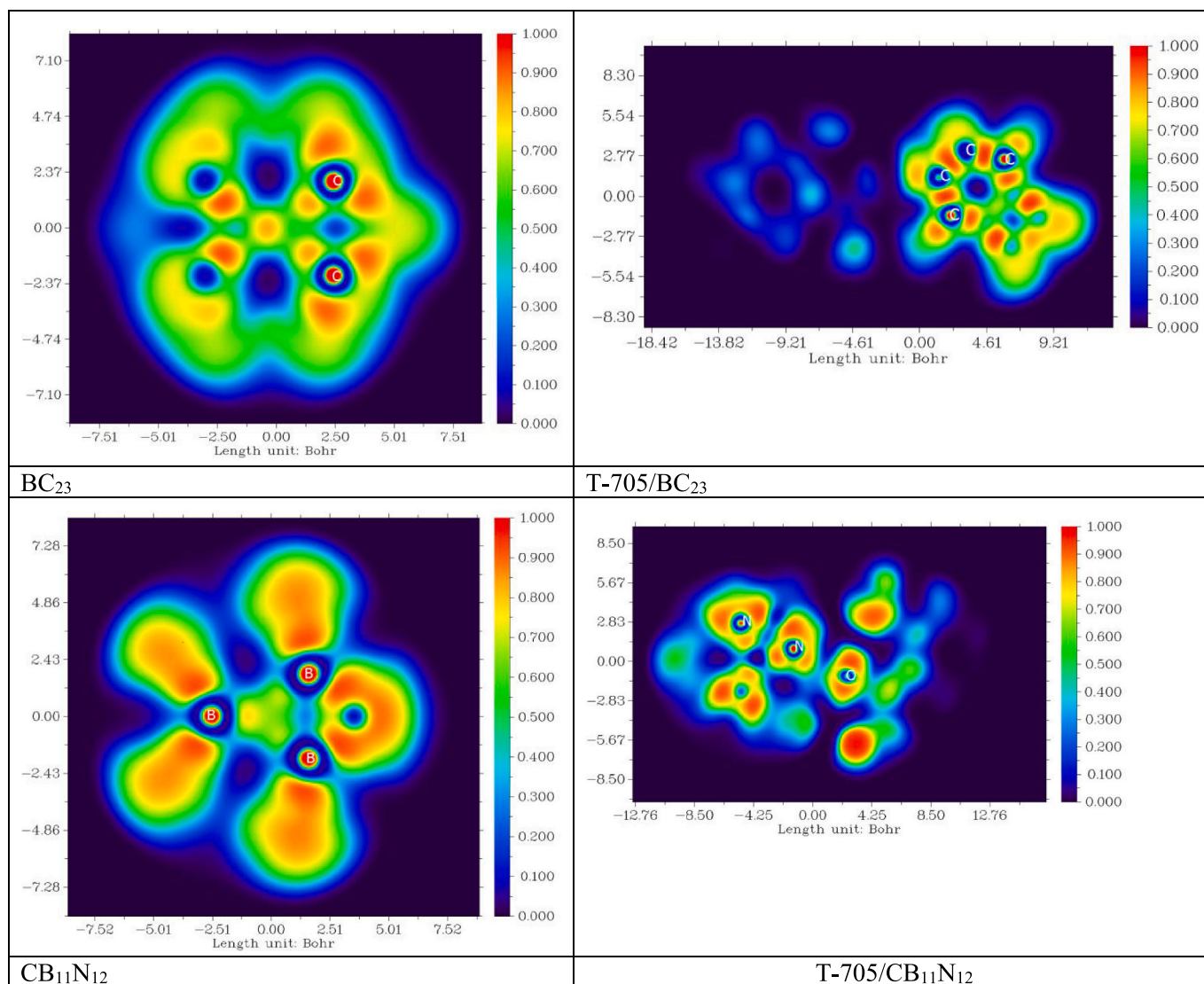
**Fig. 8.** ELF of the doped nanocages and complexes.

$BC_{23}$, $B_{12}N_{12}$, and $CB_{11}N_{12}$ sites. it is observed that a low-intensity vibrational frequency associated with the interaction of Favipiravir with $C_{24}$, $BC_{23}$, $B_{12}N_{12}$, and $CB_{11}N_{12}$ sites complex.

## 4. Conclusions

The computational calculations were conducted to characterize the mechanism of the interaction between the drug 5-Fluoro-2-hydroxypyr-azine-3-carboxamide (T-705) and $C_{24}$, BC23, $B_{12}N_{12}$, and $CB_{11}N_{12}$ based nanocarriers using the density functional theory (DFT) and the time-dependent density functional theory (TD-B3LYP and TD-CAM-B3LYP). Adsorption properties of these complexes: geometry optimization, molecular structure, MEP, spectroscopic (UV/Vis, excited State and IR), and the thermodynamic parameters have been examined. Interestingly, the presence of nanocage does not induce any major structural deformation in the T-705, and the incorporation of heteroatoms in perfect $C_{24}$ and $B_{12}N_{12}$ (BC23 and $CB_{11}N_{12}$) nanocages exhibits comparatively higher interacting energies compared to perfect nanocage. Moreover, the energy gap of $CB_{11}N_{12}$ drastically lowers by 2.31 eV, Indicating increase in reactivity and a decrease in stability. For the T-705/$CB_{11}N_{12}$ complexes, the excitation from the HOMO to LUMO. The reduction of the energy gap of excited-state showed that the $\lambda_{max}$ was red-shifted by 79 nm.

MEP predict the electrophilic and nucleophilic sites and NBO analysis explored the charge transfer within different orbitals in the studied complexes. The projected density of states (PDOS) of these complexes without and with solvent has been explained to examine the role of water in the interaction of T-705 with $C_{24}$, $B_{12}N_{12}$, BC23 and $CB_{11}N_{12}$ nanoparticles. The essence of interaction between T-705 drug and nanocage is explored by NCI which illustrated that weak interaction between drug molecule and the nanocage. The change in electron density after drug adsorption on nanocage is investigated by ELF maps.

The two different temperatures (298.15 to 310.15 K) were examine for the interaction of T-705 molecule with $B_{12}N_{12}$, $CB_{11}N_{12}$, $C_{24}$, BC23 in the gas and aqueous. The derived thermodynamic parameters of T-705@ $BC_{23}$, T-705@ $B_{12}N_{12}$ and T-705@ $CB_{11}N_{12}$ with negative $\Delta G$ implying the spontaneity of the interaction. Consequently, the $BC_{23}$, $B_{12}N_{12}$, and $CB_{11}N_{12}$ nanocages can be utilized as promising drug delivery vehicle for a potential antiviral T-705. T-705 can be considered a highly promising antiviral drug for COVID-19.

## CRediT authorship contribution statement

**K. A. Soliman** conceived of the idea, writing-original draft of the manuscript and reviewed it. **S. Abdel Aal** writing-original draft of the manuscript and reviewed it.

**Table 6**
Natural bond orbital analysis for The donor–acceptor interactions and second-order perturbation energies ($E^{(2)}$, kcal mol$^{-1}$) related to charge transfer between T-705 and $C_{24}$, $C_{23}B$, $B_{12}N_{12}$, $CB_{11}N_{12}$ in complexes.

| | Donor (i) | Acceptor (j) | $E^{(2)}$ | E(j) − E(i) | F(i, j) |
|---|---|---|---|---|---|
| T-705/$C_{24}$ | Π (C26-O25) | Π* (C3-C5) | 0.06 | 2.05 | 0.047 |
| | Π (C26-O25) | Π* (C3-C5) | 0.06 | 0.39 | 0.023 |
| | LP (O25) | Π* (C2-C19) | 0.99 | 0.27 | 0.040 |
| | σ (C30-C26) | σ* (C26-O25) | 0.54 | 1.26 | 0.019 |
| | σ (C30-N31) | σ* (C26-O25) | 1.35 | 1.46 | 0.047 |
| | Π (C26-O25) | Π* (C26-O25) | 1.01 | 0.37 | 0.041 |
| | LP (O25) | σ* (C26-N27) | 2.33 | 1.15 | 0.010 |
| | LP (O25) | σ* (C30-C26) | 1.91 | 1.06 | 0.005 |
| | Π* (C37-C30) | Π* (C26-O25) | 83.07 | 0.03 | 0.005 |
| | LP (O25) | σ* (C26-N27) | 2.33 | 1.15 | 0.015 |
| T-705/$C_{23}B$ | σ(C26-O25) | σ* (B3) | 20.06 | 1.17 | 0.201 |
| | LP (O25) | σ* (B3) | 9.23 | 0.58 | 0.101 |
| | LP (O25) | σ* (C2-B3) | 1.85 | 0.85 | 0.051 |
| | LP (O25) | σ* (B3) | 153.22 | 0.67 | 0.410 |
| | LP (O25) | σ* (C5-B3) | 2.10 | 0.75 | 0.055 |
| | LP (O25) | σ* (C4-B3) | 1.75 | 0.74 | 0.050 |
| | σ (C2-B3) | σ*(N27-H28) | 1.22 | 0.89 | 0.042 |
| | Π (C5-C6) | LP* (B3) | 9.53 | 0.35 | 0.074 |
| | σ (C5-B3) | Π*(C17-C8) | 1.01 | 0.59 | 0.033 |
| | σ (C7-C12) | σ* (C4-B3) | 1.42 | 1.00 | 0.048 |
| | Π (C7-C4) | Π* (B3) | 6.11 | 0.34 | 0.060 |
| | σ (C6-C10) | σ* (C5-B3) | 1.67 | 1.00 | 0.052 |
| | σ (C24-C19) | σ*(C2-B3) | 1.40 | 0.97 | 0.047 |
| | σ (C19-C2) | σ*(C2-B3) | 1.02 | 1.07 | 0.042 |
| | Π (C19-C2) | LP* (B3) | 5.33 | 0.35 | 0.057 |
| | Π (C19-C2) | σ* (C2-B3) | 1.14 | 0.63 | 0.036 |
| | σ (C4-B3) | σ*(C7-C4) | 1.74 | 1.05 | 0.055 |
| | σ (C4-B3) | σ* (C18-C1) | 3.42 | 1.00 | 0.075 |
| T-705/$B_{12}N_{12}$ | σ (B6-O25) | RY*1 (C26) | 3.26 | 1.67 | 0.066 |
| | σ (B6-O25) | RY*4 (C26) | 0.51 | 3.13 | 0.036 |
| | σ (B6-O25) | σ*(B6-N19) | 0.63 | 1.23 | 0.025 |
| | σ (B6-O25) | σ*(B6-N20) | 1.03 | 1.16 | 0.031 |
| | σ (B6-O25) | σ*(C30-C26) | 5.22 | 1.19 | 0.071 |
| | σ (B6-O25) | σ*(C26-O25) | 17.38 | 1.28 | 0.037 |
| | Π (B7-N19) | σ*(B6-O25) | 13.26 | 0.58 | 0.080 |
| | σ (C30-C26) | σ*(B6-O25) | 4.19 | 1.01 | 0.059 |
| | σ(C26-O25) | σ*(B6-O25) | 1.63 | 1.32 | 0.042 |
| | LP (N17) | σ*(B6-O25) | 8.25 | 0.56 | 0.064 |
| | LP (N20) | σ*(B6-O25) | 12.07 | 0.54 | 0.078 |
| | LP (O25) | σ* (B6) | 131.59 | 1.70 | 0.047 |
| T-705/$CB_{11}N_{12}$ | σ (N19-B6) | σ* (C26-O25) | 0.57 | 1.11 | 0.032 |
| | σ (N20-B6) | σ* (C26-O25) | 0.29 | 1.04 | 0.022 |
| | σ (N20-B6) | Π* (C26-O25) | 0.31 | 0.50 | 0.018 |
| | σ (C30-N31) | σ* (C26-O25) | 0.92 | 1.36 | 0.045 |
| | σ (C26-O25) | σ* (O25-B6) | 0.80 | 1.32 | 0.042 |
| | Π (C26-O25) | σ* (N19-B6) | 1.14 | 0.84 | 0.039 |
| | σ (C26-O25) | σ* (N20-B6) | 15.34 | 0.78 | 0.051 |
| | LP (O25) | LP* (B6) | 18.68 | 1.74 | 0.044 |
| | LP (O25) | σ* (N17-B6) | 98.19 | 0.78 | 0.052 |
| | LP (O25) | σ* (N19-B6) | 0.93 | 0.90 | 0.037 |
| | LP (O25) | σ* (O25-B6) | 0.25 | 0.76 | 0.018 |
| | σ* (O25-B6) | σ*(C26-O25) | 1.66 | 0.18 | 0.087 |
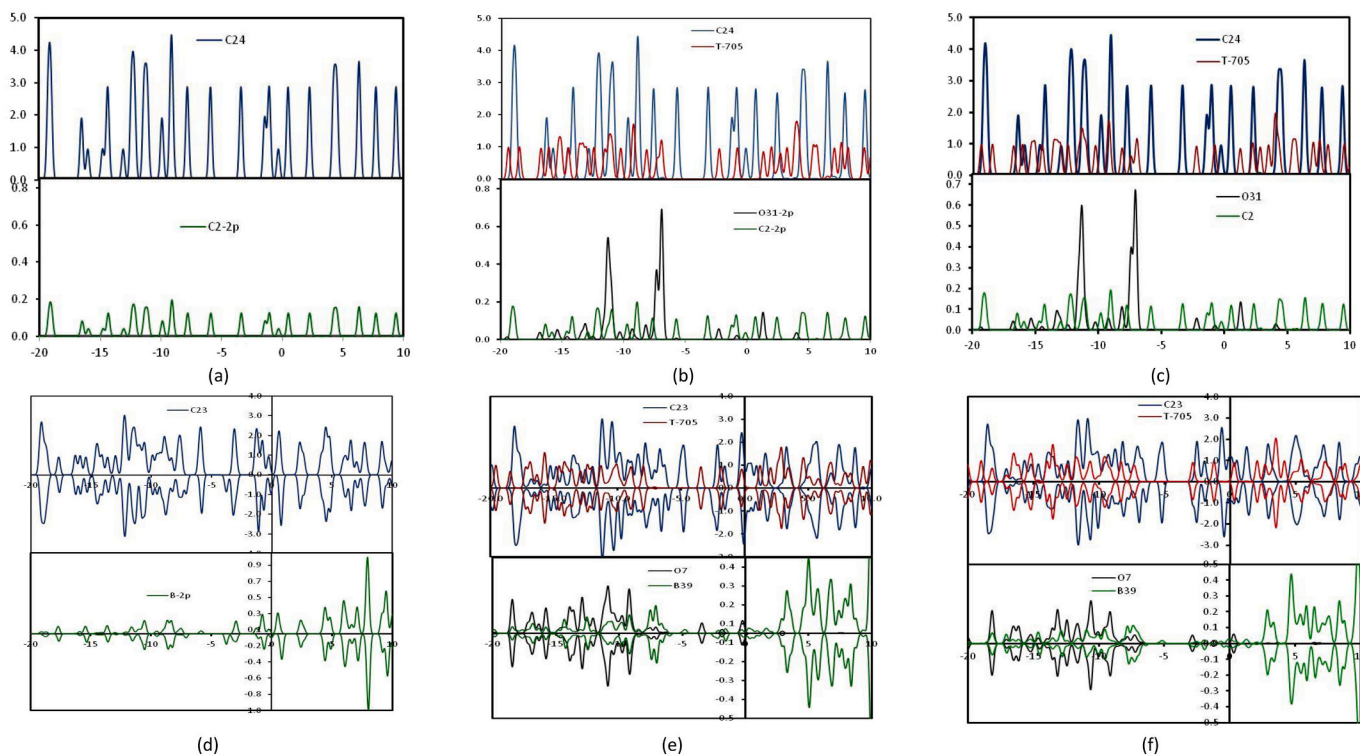
**Fig. 9.** The projected density of states (PDOS) of (a) $C_{24}$ (b)T-705/$C_{24}$ in gas phase, (c) T-705/$C_{24}$ in aqueous phase (d) $C_{23}B$, (e) T-705/$C_{23}B$ in gas phase and (f) T-705/$C_{23}B$ in aqueous phase. The Fermi level is set to be 0.
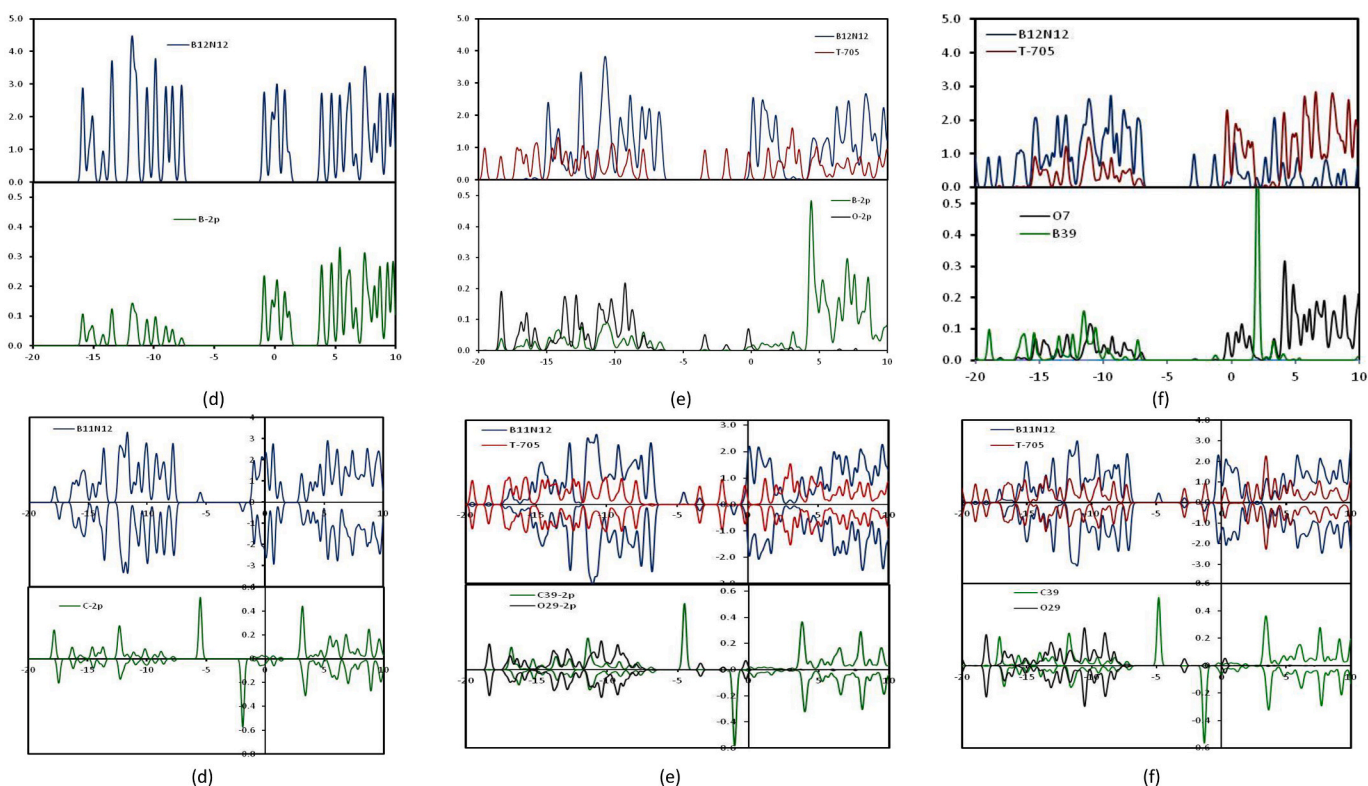


**Fig. 10.** The projected density of states (PDOS) of (a) $B_{12}N_{12}$ (b) T-705/$B_{12}N_{12}$ in gas phase, (c) T-705/$B_{12}N_{12}$ in aqueous phase (d) $CB_{11}N_{12}$, (e) T-705/$CB_{11}N_{12}$ in gas phase and (f) T-705/ $CB_{11}N_{12}$ in in aqueous phase. The Fermi level is set to be 0.

**Table 7**

Selected excitation energies (E, eV), wavelength (λ, nm) oscillator strength (f), and relative orbital contributions calculated for the most stable configuration of T-705, $C_{24}$, $BC_{23}$, $B_{12}N_{12}$ and $CB_{11}N_{12}$ nanocages in the gas and aqueous phase using B3LYP approximations.

| Gas phase | | | | | Aqueous phase | | | | |
|---|---|---|---|---|---|---|---|---|---|
| Structure | E | λ | f | MO contributions | Structure | E | λ | f | MO contributions |
| T-705 | 4.3144 | 287.37 | 0.1088 | HOMO→LUMO (98%) | T-705 | 4.2852 | 289.33 | 0.1819 | HOMO→LUMO (94%) |
| | 5.9429 | 208.63 | 0.1460 | H-5 → LUMO (11%), H-1 → L + 1 (79%), H-2 → L + 1 (7%) | | 5.8746 | 211.05 | 0.1591 | HOMO→L + 1 (88%), H-5 → LUMO (9%) |
| | 6.8316 | 181.49 | 0.1803 | H-5 → LUMO (78%), H-9 → LUMO (4%), H-6 → LUMO (4%), H-1 → L + 1 (8%), | | 6.7875 | 182.67 | 0.2341 | H-5 → LUMO (82%), H-6 → LUMO (3%), HOMO→L + 1 (8%) |
| | 7.5955 | 163.23 | 0.1420 | H-5 → L + 1 (19%), H-1 → L + 2 (73%) | | 7.4814 | 165.72 | 0.1557 | H-5 → L + 1 (16%), HOMO→L + 2 (78%) |
| $C_{24}$ | 3.7436 | 331.19 | 0.0182 | H-4 → L + 2 (17%), H-3 → LUMO (26%), H-2 → L + 6 (11%) | $C_{24}$ | 3.7362 | 331.84 | 0.0228 | H-5 → LUMO (12%), H-4 → L + 1 (15%), H-4 → L + 2 (14%), H-3 → LUMO (10%) |
| $C_{23}B$ | 2.3913 | 518.47 | 0.0104 | H-2(B) → LUMO(B) (78%), H-3(A) → L + 2 (A) (4%),HOMO(A) → L + 2(A) (3%) | $C_{23}B$ | 2.3772 | 521.54 | 0.0141 | H-2(B) → LUMO(B) (78%), H-3(A) → LUMO(A) (2%), H-3(A) → L + 2(A) (3%) |
| $B_{12}N_{12}$ | 6.4762 | 191.45 | 0.0336 | H-1 → L + 3 (36%), HOMO→L + 4 (16%), H-4 → L + 2 (9%), H-3 → LUMO (3%), H-3 → L + 2 (6%) | $B_{12}N_{12}$ | 6.5100 | 190.45 | 0.0470 | H-1 → L + 3 (36%), HOMO→L + 4 (22%), H-4 → LUMO (5%), H-3 → L + 2 (9%), |
| $CB_{11}N_{12}$ | 5.7400 | 216.00 | 0.0131 | H-4(B) → LUMO(B) (74%), H-2(A) → L + 2 (A) (2%), HOMO(A) → L + 11(A) (9%), H-1 (B) → LUMO(B) (3%) | $CB_{11}N_{12}$ | 5.7120 | 217.06 | 0.0230 | H-4(B) → LUMO(B) (85%), H-1(B) → LUMO(B) (3%), H-1(B) → L + 3(B) (3%) |
| | 4.5481 | 272.61 | 0.0116 | HOMO(A) → L + 5(A) (84%), HOMO(A) → L + 2(A) (8%), HOMO(A) → L + 9(A) (3%) | | 4.6087 | 269.02 | 0.0162 | HOMO(A) → L + 5(A) (82%), HOMO (A) → L + 2(A) (8%), HOMO(A) → L + 9(A) (3%). |

**Table 8**

Selected excitation energies (E, eV), wavelength (λ, nm) oscillator strength (f), and relative orbital contributions calculated for the most stable configuration of T-705/$C_{24}$, T-705/$C_{23}B$, T-705/$B_{12}N_{12}$ and T-705/$CB_{11}N_{12}$ complexes in the gas and aqueous phase using B3LYP approximations.

| Gas phase | | | | | Aqueous phase | | | | |
|---|---|---|---|---|---|---|---|---|---|
| Structure | E | λ | f | MO contributions | Structure | E | λ | f | MO contributions |
| T-705/$C_{24}$ | 3.2109 | 386.13 | 0.0592 | H-3 → LUMO (15%), H-3 → L + 1 (56%), H-3 → L + 2 (27%) | T-705/$C_{24}$ | 3.2527 | 381.17 | 0.0072 | H-4 → LUMO (48%), H-4 → L + 1 (13%), H-4 → L + 2 (29%), H-8 → L + 1 (3%), H-3 → LUMO (3%) |
| T-705/$C_{23}B$ | 2.1677 | 571.96 | 0.0014 | HOMO(A) → L + 4(A) (33%), H-2(B) → LUMO(B) (55%), H-2(B) → L + 1(B) (3%), HOMO(B) → L + 5(B) (3%) | T-705/$C_{23}B$ | 2.1994 | 563.71 | 0.0015 | H-2(A) → LUMO(A) (47%), H-2(A) → L + 1(A) (18%), H-1(B) → L + 4(B) (12%) |
| T-705/$B_{12}N_{12}$ | 4.1363 | 299.75 | 0.1837 | H-3 → LUMO (74%), H-6 → LUMO (18%), H-8 → LUMO (5%) | T-705/$B_{12}N_{12}$ | 4.0621 | 305.22 | 0.2867 | H-2 → LUMO (97%) |
| T-705/$CB_{11}N_{12}$ | 3.7641 | 329.38 | 0.0032 | H-3(A) → LUMO(A) (88%), H-12(A) → LUMO(A) (2%), H-12(B) → LUMO(B) (2%) | T-705/$CB_{11}N_{12}$ | 4.0432 | 306.65 | 0.2600 | H-2(A) → LUMO(A) (50%), H-3(B) → LUMO(B) (44%), H-4(A) → LUMO(A) (2%) |

**Table 9**

Selected excitation energies (E, eV), wavelength ($\lambda$, nm) oscillator strength (f), and relative orbital contributions calculated for the most stable configuration of T-705, $C_{24}$, $BC_{23}$, $B_{12}N_{12}$ and $CB_{11}N_{12}$ nanocages in the gas and aqueous phase using CAM-B3LYP approximations.

| Gas phase | | | | | Aqueous phase | | | | |
|---|---|---|---|---|---|---|---|---|---|
| Structure | E | $\lambda$ | f | MO contributions | Structure | E | $\lambda$ | f | MO contributions |
| T-705 | 4.1240 | 300.64 | 0.0017 | H-1(A) → LUMO(A) (44%), H-1(B) → LUMO(B) (44%) | | 4.3214 | 286.91 | 0.0028 | H-1(A) → LUMO(A) (43%), H-1(B) → LUMO(B) (43%) |
| | 4.5547 | 272.21 | 0.1749 | H-2(A) → LUMO(A) (37%), H-2(B) → LUMO(B) (37%) | | 4.4953 | 275.81 | 0.2202 | HOMO(A) → LUMO(A) (48%), HOMO(B) → LUMO(B) (48%) |
| | 5.4011 | 229.56 | 0.0212 | H-2(A) → LUMO(A) (49%), H-2(B) → LUMO(B) (49%) | | 5.5953 | 221.59 | 0.0340 | H-2(A) → LUMO(A) (49%), H-2(B) → LUMO(B) (49%) |
| | 6.1749 | 200.79 | 0.1395 | HOMO(A) → L + 1(A) (43%), HOMO(B) → L + 1(B) (43%) | | 6.1103 | 202.91 | 0.1690 | HOMO(A) → L + 1(A) (43%), HOMO(B) → L + 1(B) (43%) |
| $C_{24}$ | 4.2472 | 291.92 | 0.0462 | H-2 → L + 4 (10%), HOMO→L + 3 (32%), HOMO→L + 4 (13%) | | 4.2037 | 292.562 | 0.0589 | H-2 → L + 4 (11%), HOMO→L + 3 (34%), HOMO→L + 4 (15%) |
| $C_{23}B$ | 2.9533 | 419.82 | 0.0070 | H-1(A) → L + 1(A) (21%), H-2(B) → LUMO(B) (37%) | | 2.9468 | 420.74 | 0.0104 | H-1(A) → L + 1(A) (17%), H-2(B) → LUMO(B) (41%) |
| $B_{12}N_{12}$ | 6.3118 | 193.50 | 0.0231 | H-1 → L + 3 (34%), HOMO→L + 4 (17%), H-4 → L + 2 (11%), | $B_{12}N_{12}$ | 6.7057 | 192.43 | 0.0358 | H-1 → L + 3 (34%), HOMO→L + 4 (21%), H-4 → LUMO (9%) |
| $CB_{11}N_{12}$ | 5.3745 | 230.69 | 0.0146 | H-4(B) → LUMO(B) (10%), H-1(B) → LUMO(B) (78%) | | 5.3533 | 231.60 | 0.0184 | H-4(B) → LUMO(B) (10%), H-1(B) → LUMO(B) (74%) |
| | 4.4042 | 281.52 | 0.0007 | HOMO(A) → LUMO(A) (84%), HOMO(A) → L + 6(A) (11%) | | 4.4665 | 277.59 | 0.0009 | HOMO(A) → LUMO(A) (84%), HOMO(A) → L + 6(A) (11%) |

**Table 10**

Selected excitation energies (E, eV), wavelength ($\lambda$, nm) oscillator strength (f), and relative orbital contributions calculated for the most stable configuration of T-705/$C_{24}$, T-705/$C_{23}B$, T-705/$B_{12}N_{12}$ and T-705/$CB_{11}N_{12}$ complexes in the gas and aqueous phase using CAM-B3LYP approximations.

| Gas phase | | | | | Aqueous phase | | | | |
|---|---|---|---|---|---|---|---|---|---|
| Structure | E | $\lambda$ | f | MO contributions | Structure | E | $\lambda$ | f | MO contributions |
| T-705/$C_{24}$ | 4.2502 | 291.71 | 0.0536 | H-2 → L + 4 (19%), H-2 → L + 5 (26%), HOMO→L + 5 (20%) | T-705/$C_{24}$ | 3.0527 | 387.20 | 0.0011 | H-3 → LUMO (36%), H-2 → L + 1 (13%), H-3 → L + 2 (29%) |
| T-705/$C_{23}B$ | 2.4801 | 499.91 | 0.0013 | HOMO(A) → LUMO(A) (79%) | T-705/$C_{23}B$ | 2.5204 | 491.92 | 0.0037 | HOMO(A) → L + 2(A) (82%) |
| T-705/$B_{12}N_{12}$ | 4.3493 | 285.06 | 0.2057 | H-6(A) → LUMO(A) (21%), HOMO(A) → LUMO(A) (18%), H-6(B) → LUMO(B) (21%), HOMO(B) → LUMO(B) (18%) | T-705/$B_{12}N_{12}$ | 4.3215 | 289.06 | 0.3890 | H-5(A) → LUMO(A) (22%), HOMO(A) → LUMO(A) (19%), H-6(B) → LUMO(B) (23%), |
| T-705/$CB_{11}N_{12}$ | 4.3718 | 283.60 | 0.2738 | H-6(A) → LUMO(A) (39%), H-6(B) → LUMO(B) (16%), H-5(B) → LUMO(B) (26%) | T-705/$CB_{11}N_{12}$ | 4.2919 | 288.88 | 0.3420 | H-2(A) → LUMO(A) (27%), H-1(A) → LUMO(A) (21%), H-2(B) → LUMO(B) (21%), H-1(B) → LUMO(B) (25%) |
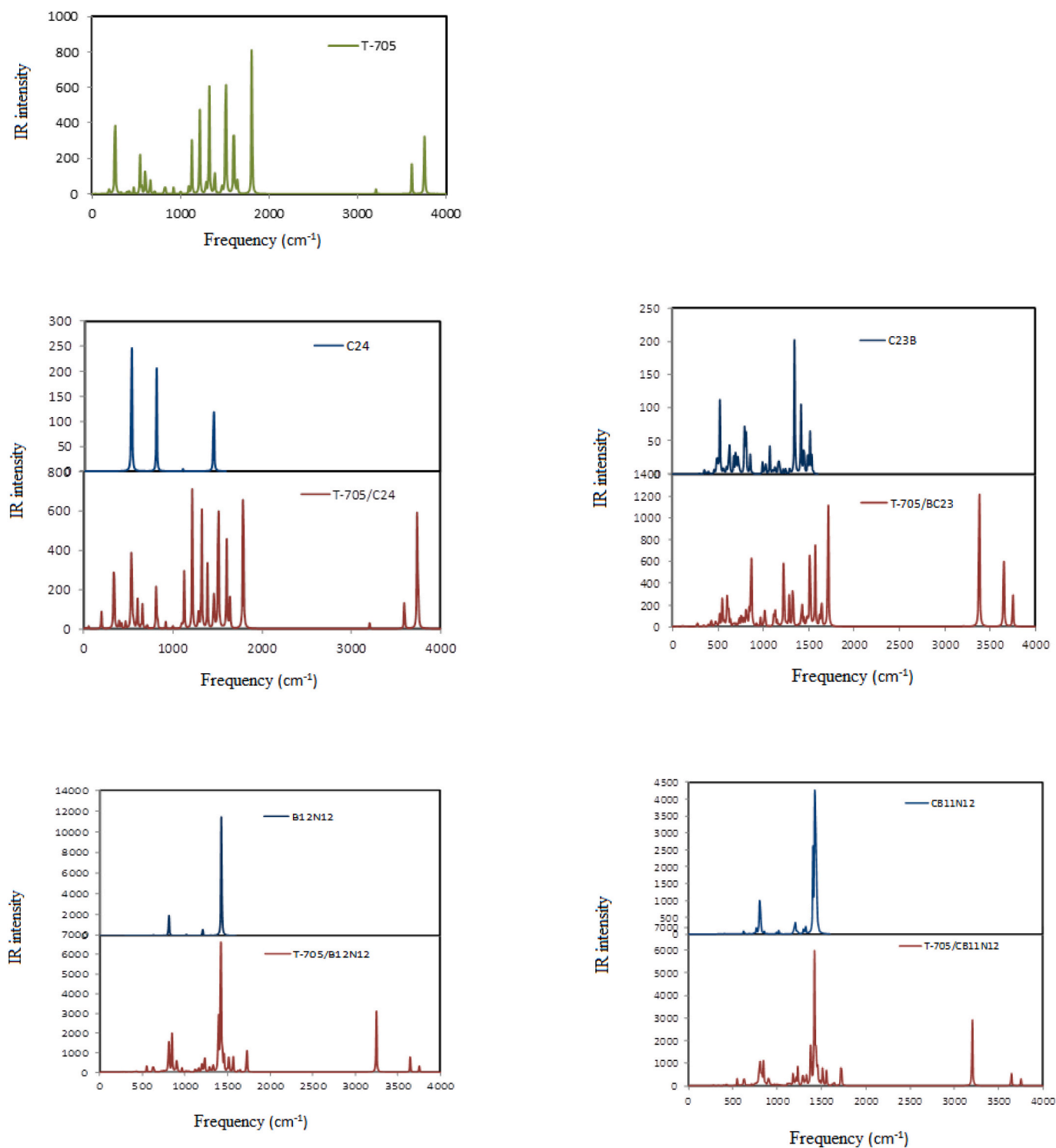
**Fig. 11.** IR spectra of T-705, nanocages and their complexes.

## Declaration of competing interest

The authors declare no conflict of interest.

## Appendix A. Supplementary data

Supplementary data to this article can be found online at https://doi.org/10.1016/j.diamond.2021.108458.

## References

[1] A.E. Allam, H.K. Assaf, H.A. Hassan, K. Shimizuc, A.M.M. Elshaier, An in silico perception for newly isolated flavonoids from peach fruit as privileged avenue for a countermeasure outbreak of COVID-19, RSC Adv. 10 (2020) 29983–29998.

[2] Y. Furuta, K. Takahashi, K. Shiraki, K. Sakamoto, D.F. Smee, D.L. Barnard, B. B. Gowen, J.G. Julander, J.D. Morrey, T-705 (favipiravir) and related compounds: Novel broad-spectrum inhibitors of RNA viral infections, Antiviral Res. 82 (2009) 95–102.

[3] Y. Furuta, B. Gowen, K. Takahashi, K. Shiraki, D.F. Smee, D.L. Barnard, Favipiravir (T-705), a novel viral RNA polymerase inhibitor, Antiviral Res. 100 (2013) 446–454.

[4] L. Caly, J.D. Druce, M.G. Catton, D.A. Jans, K.M. Wagstaff, The FDA-approved drug ivermectin inhibits the replication of SARS-CoV-2 in vitro, Antivir. Res. 178 (2020) 104787.

[5] L. Rhyman, M. Tursun, H.H. Abdallah, Y.S. Choong, C. Parlak, P. Kharkar, P. Ramasami, Theoretical investigation of the derivatives of favipiravir (T-705) as potential drugs for Ebola virus, Phys. Sci. Rev. 20170198 (2018).

[6] F.Y. Shi, Z.T. Li, L.J. Kong, Y.C. Xie, T. Zhang, W.F. Xu, Synthesis and crystal structure of 6-fluoro-3-hydroxypyrazine-2-carboxamide, Drug Discov. Ther. 8 (2014) 117–120.

[7] D. Buttler, Ebola drug trials set to begin amid crisis, Nature. 513 (2014) 156.

[8] P.M. Tiwari, K. Vig, V.A. Dennis, R. Shree, Functionalized gold nanoparticles and their biomedical applications, Nanomaterials. 1 (2011) 31–63.

[9] Y. Wang, Z. Xu, Interaction mechanism of doxorubicin and SWCNT: protonation and diameter effects on drug loading and releasing, RSC Adv. 6 (2016) 314–322.

[10] K. Seino, W.G. Schmidt, Reflectance anisotropy of uracil covered Si(0 0 1) surfaces: Ab initio predictions, Surf. Sci. 548 (2004) 183–186.

[11] E. Duverger, T. Gharbi, E. Delabrousse, F. Picaud, Quantum study of boron nitride nanotubes functionalized with anticancer molecules, Phys. Chem. Chem. Phys. 16 (2014) 18425–18432.

[12] L. Ci, L. Song, C. Jin, D. Jariwala, D. Wu, Y. Li, A. Srivastava, Z.F. Wang, K. Storr, L. Balicas, F. Liu, P.M. Ajayan, Atomic layers of hybridized boron nitride and graphene domains, Nat. Mater. 9 (2010) 430–435.

[13] B. Guo, L. Fang, B. Zhan, J.R. Gong, Graphene doping: a review, Insci. J. 1 (2011) 80–89.

[14] A. Hosseinian, E. Vessally, S. Yahyaei, L. Edjlali, A. Bekhradnia, A density functional theory study on the interaction between 5-fluorouracil drug and C24 fullerene, J. Clust. Sci. 28 (2017) 2681–2692.

[15] M.K. Hazrati, N.L. Hadipour, Adsorption behavior of 5-fluorouracil on pristine, B-, Si-, and Al-doped C60 fullerenes: a first-principles study, Phys. Lett. A 380 (2016) 937–941.

[16] W.L. Wang, Y. Bando, C.Y. Zhi, W.F. Fu, E.G. Wang, D. Golberg, Aqueous noncovalent functionalization and controlled near-surface carbon doping of multiwalled boron nitride nanotubes, J. Am. Chem. Soc. 130 (2008) 8144–8145.

[17] G. Ciofani, V. Raffa, A. Mencissi, P. Dario, Preparation of boron nitride nanotubes aqueous dispersions for biological applications, J. Nanosci. Nanotechnol. 8 (2008) 6223–6231.

[18] C.Y. Zhi, J.L. Zhang, Y. Bando, T. Terao, C.C. Tang, H. Kuwahara, D. Golberg, New crystalline phase induced by boron nitride nanotubes in polyaniline, J. Phys. Chem. C 112 (2008) 17592–17595.

[19] G. Ciofani, V. Raffa, A.J. Yu, Y. Chen, Y. Obata, S. Takeoka, A. Mencissi, A. Cuschieri, Boron nitride nanotubes: a novel vector for targeted magnetic drug delivery, Curr. Nanosci. 5 (2009) 33–38.

[20] A. Soltani, A. Sousaraei, M. Bezi Javan, M. Eskandaric, H. Balakheyli, Electronic and optical properties of 5-AVA-functionalized BN nanoclusters: a DFT study, New J. Chem. 40 (2016) 7018–7026.

[21] D.V. Shtansky, K.L. Firestein, D.V. Golberg, Fabrication and application of BN nanoparticles, nanosheets and their nanohybrids, Nanoscale. 10 (2018) 17477–17493.

[22] B.T. Tomic, C.S. Abraham, S. Pelemis, S.J. Armakovic, S. Armakovic, Fullerene C24 as a potential carrier of ephedrine drug – a computational study of interactions and influence of temperature, Phys. Chem. Chem. Phys. 21 (2019) 23329–23337.

[23] A. Goyal, D. Aggarwal, S. Kapoor, N. Goel, S. Singhal, J. Shukl, A comprehensive experimental and theoretical study on BN nanosheets for the adsorption of pharmaceutical drugs, New J. Chem. 44 (2020) 3985–3997.

[24] S. Mourdikoudis, R.M. Pallares, N.T.K. Thanh, Characterization techniques for nanoparticles: comparison and complementarity upon studying nanoparticle properties, Nanoscale. 10 (2018) 12871–12934.

[25] C. Parlak, Ö. Alver, M. Şenyel, Computational study on favipiravir adsorption onto undoped- and silicon-decorated C60 fullerenes, J. Theor. Comput. Chem. 16 (2017) 1750011.

[26] A.S. Rad, M. Ardjmand, M.R. Esfahani, B. Khodashenas, DFT calculations towards the geometry optimization, electronic structure, infrared spectroscopy and UV–vis analyses of Favipiravir adsorption on the first-row transition metals doped fullerenes; a new strategy for COVID-19 therapy, Spectrochim. Acta A Mol. Biomol. Spectrosc. 247 (2021) 119082.

[27] Y. Takano, K.N. Houk, Benchmarking the conductor-like polarizable continuum model (CPCM) for aqueous solvation free energies of neutral and ionic organic molecules, J. Chem. Theory Comput. 1 (2005) 70–77.

[28] A. Soltani, M.T. Baei, A.S. Ghasemi, K.H. Amirabadi, Adsorption of cyanogen chloride over Al- and Ga-doped BN nanotubes, Superlattice. Microst. 75 (2014) 564–575.

[29] A. Soltani, M.T. Baei, E.T. Lemeski, A.A. Pahlevani, The study of SCN⁻ adsorption on $B_{12}N_{12}$ and $B_{16}N_{16}$ nano-cages, Superlattice. Microst. 75 (2014) 716–724.

[30] O.A. El-Gammal, T.H. Rakha, H.M. Metwally, G.M. Abu El-Reash, Synthesis, characterization, DFT and biological studies of isatinpicolinohydrazone and its Zn (II), Cd(II) and Hg(II) complexes, Spectrochim. Acta A. 127 (2014) 144–156.

[31] A. Tariq, S. Nazir, A.W. Arshad, F. Nawaz, K. Ayub, J. Iqbal, DFT study of the therapeutic potential of phosphorene as a new drug-delivery system to treat cancer, RSC Adv. 9 (2019) 24325–24332.

[32] M. Sheikhi, S. Shahab, M. Khaleghian, R. Kumar, Interaction between new anti-cancer drug Syndros and CNT(6,6-6) nanotube for medical applications: geometry optimization, molecular structure, spectroscopic (NMR, UV/Vis, excited state), FMO, MEP and HOMO-LUMO investigation, Appl Surf Sci 434 (2018) 504–513.

[33] T. Yanai, D.P. Tew, N.C. Handy, A new hybrid exchange–correlation functional using the coulomb-attenuating method (CAM-B3LYP), Chem. Phys. Lett. 393 (2004) 51–57.

[34] K.B. Petrushenko, I.K. Petrushenko, O.V. Petrova, L.N. Sobenina, I.A. Ushakov, B. A. Trofimov, Environment-responsive 8-CF3-BODIPY dyes with aniline groups at the 3 position: synthesis, optical properties and RI-CC2 calculations, Asian J. Org Chem. 6 (2017) 852–861.

[35] M.J.G. Peach, P. Benfield, T. Helgaker, D.J. Tozer, Excitation energies in density functional theory: an evaluation and a diagnostic test, J. Chem. Phys. 128 (2008), 044118.

[36] I.K. Petrushenko, K.B. Petrushenko, Effect of methyl substituents on the electronic transitions in simplemeso-aniline-BODIPY based dyes: RI-CC2 and TD-CAM-B3LYP computational investigation, Spectrochim. Acta A Mol. Biomol. Spectrosc. 190 (2018) 239–245.

[37] M.J. Frisch, G.W. Trucks, H.B. Schlegel, G.E. Scuseria, M.A. Robb, J.R. Cheeseman, G. Scalmani, V. Barone, B. Mennucci, G.A. Petersson, H. Nakatsuji, M. Caricato, X. Li, H.P. Hratchian, A.F. Izmaylov, J. Bloino, G. Zheng, J.L. Sonnenberg, M. Hada, M. Ehara, K. Toyota, R. Fukuda, J. Hasegawa, M. Ishida, T. Nakajima, Y. Honda, O. Kitao, H. Nakai, T. Vreven, J.A. Montgomery, J.E. Peralta, F. Ogliaro, M. Bearpark, J.J. Heyd, E. Brothers, K.N. Kudin, V.N. Staroverov, R. Kobayashi, J. Normand, K. Raghavachari, A. Rendell, J.C. Burant, S.S. Iyengar, J. Tomasi, M. Cossi, N. Rega, J.M. Millam, M. Klene, J.E. Knox, J.B. Cross, V. Bakken, C. Adamo, J. Jaramillo, R. Gomperts, R.E. Stratmann, O. Yazyev, A.J. Austin, R. Cammi, C. Pomelli, J.W. Ochterski, R.L. Martin, K. Morokuma, V.G. Zakrzewski, G.A. Voth, P. Salvador, J.J. Dannenberg, S. Dapprich, A.D. Daniels, Farkas, J. B. Foresman, J.V. Ortiz, J. Cioslowski, D.J. Fox, Gaussian 09, Gaussian, Inc., Wallingford CT, 2009.

[38] N.M. O'Boyle, A.L. Tenderholt, K.M. Langner, cclib: A library for package-independent computational chemistry algorithms, J. Comput. Chem. 29 (2008) 839–845.

[39] M. Shahid, M. Salim, M. Khalid, M.N. Tahir, M.U. Khan, A.A.C. Braga, Synthetic, XRD, non-covalent interactions and solvent dependent nonlinear optical studies of sulfadiazine-Ortho-vanillin Schiff base: (E)-4-((2-hydroxy-3-methoxy- benzylidene) amino)-N-(pyrimidin-2-yl)benzene-sulfonamide, J. Mol. Struct. 1161 (2018) 66–75.

[40] N. Saikia, R.C. Deka, Density functional study on noncovalent functionalization of pyrazinamide chemotherapeutic with graphene and its prototypes, New J.Chem. 38 (2014) 1116–1128.

[41] A. Ashraf, M. Khalid, M.N. Tahir, M. Yaqub, M.M. Naseer, G.M. Kamal, B. Saifullah, A.A.C. Braga, Z. Shafiq, W. Rauf, A facile and concise route to (hydroxybenzoyl) pyrido[2,3-d]pyrimidine heterocycle derivatives: synthesis, and structural, spectral and computational exploration, RSC Adv. 9 (2019) 34567–34580.

[42] A. Soltani, M.B. Javanc, Carbon monoxide interactions with pure and doped B11XN12 (X = Mg, Ge, Ga) nano-clusters: a theoretical study, RSC Adv. 5 (2015) 90621–90631.

[43] S. Moro, M. Bacilieri, C. Ferrari, G. Spalutto, Autocorrelation of molecular electrostatic potential surface properties combined with partial least squares analysis as alternative attractive tool to generate ligand-based 3D-QSARs, Curr. Drug Discov. Technol. 2 (2005) 13–21.

[44] E.M.D. Lestard, D.M. Gil, O. Estévez-Hernández, M.F. Erben, J. Duque, Structural, vibrational and electronic characterization of 1-benzyl-3-furoyl-1-phenylthiourea: an experimental and theoretical study, New J. Chem. 39 (2015) 7459–7471.

[45] E. Scrocco, J. Tomasi, Electronic molecular structure, reactivity and intermolecular forces: an euristic interpretation by means of electrostatic molecular potentials, Adv. Quantum Chem. 11 (1979) 115–193.

[46] B. Kumar Paul, D. Ray, N. Guchhait, Unraveling the binding interaction and kinetics of a prospective anti-HIV drug with a model transport protein: results and challenges, Phys. Chem. Chem. Phys. 15 (2013) 1275–1287.

[47] A.D. Becke, K.E. Edgecombe, A simple measure of electron localization in atomic and molecular systems, J. Chem. Phys. 92 (1990) 5397.

[48] A. Soltani, M.B. Javan, M.S. Hoseininezhad-Namin, N. Tajabor, E.T. Lemeski, F. Pourarian, Interaction of hydrogen with Pd- and co-decorated C24 fullerenes: density functional theory study, Synth. Met. 234 (2017) 1–8.

[49] J. Galy, G. Couégnat, E. Vila, S.F. Matar, Stereochemistry of nitrogen E lone pair in NH3E, NOFE, N2O3E2, AgNO2E, and NCl3E, C R Chim. 20 (4) (2017) 446–459.

[50] T. Yanai, D.P. Tew, N.C. Handy, A new hybrid exchange–correlation functional using the coulomb-attenuating method (CAM-B3LYP), Chem. Phys. Lett. 393 (2004) 51–57.

[51] E.D. Glendening, J. Badenhoop, F. Weinhold, Natural resonance theory: III. Chemical applications, J. Comput. Chem. 19 (1998) 628–646.

[52] J. Foster, F. Weinhold, Natural hybrid orbitals, J. Am. Chem. Soc. 102 (1980) 7211–7218.

[53] J. Romanos, M. Beckner, D. Stalla, A. Tekeei, G. Suppes, S. Jalisatgi, M. Lee, F. Hawthorne, J.D. Robertson, L. Firlej, B. Kuchta, C. Wexler, P. Yu, P. Pfeifer, Infrared study of boron–carbon chemical bonds in boron-doped activated carbon, Carbon 54 (2013) 208–214.